CSIRO PUBLISHING

Journal of Southern Hemisphere Earth Systems Science, 2020, **70**, 304–327
https://doi.org/10.1071/ES19037

Seasonal Climate Summary

Seasonal climate summary for the southern hemisphere (spring 2017): equal-fifth warmest spring on record, with rainfall mixed

Skie Tobin

Bureau of Meteorology, GPO Box 1289, Melbourne, Vic. 3001, Australia.
Email: skie.tobin@bom.gov.au

Abstract. This is a summary of the southern hemisphere atmospheric circulation patterns and meteorological indices for spring 2017; an account of seasonal rainfall and temperature for the Australian region and the broader southern hemisphere is also provided. The tropical Pacific Ocean cooled from mid-winter, with an unusually late La Niña becoming established by the end of spring. Spring was the equal-fifth warmest on record, in terms of area-averaged national mean temperature, and was characterised by exceptional September warmth over eastern Australia, while rainfall was mixed geographically and from month-to-month, but below average overall.

Keywords: Antarctica, Australia, climate, climate drivers, ENSO, IOD, La Niña, MJO, rainfall, SAM, seasonal climate summary, seasonal summary, southern hemisphere, temperature.

Received 2 October 2019, accepted 20 January 2020, published online 17 September 2020

1 Introduction

This summary reviews the southern hemisphere and equatorial climate patterns for spring 2017, with particular attention given to the Australasian and equatorial regions of the Pacific and Indian ocean basins. The main sources of information for this report are analyses prepared by the Australian Bureau of Meteorology, the United States National Oceanic and Atmospheric Administration (NOAA) and the Global Precipitation Climatology Center (GPCC).

Unless otherwise stated, anomalies are calculated with respect to the period 1961–1990, and percentile-based analyses for the period from the start of the relevant dataset to 2017. ACORN-SAT version 2, released in December 2018 (Trewin 2018), was used in the preparation of this document; differences between the values presented herein and those published at the time, which were based on ACORN-SAT version 1 (Trewin 2013), are expected.

2 Climate drivers

2.1 El Niño–Southern Oscillation (ENSO)

The Troup Southern Oscillation Index[1] (SOI) for the period from January 2013 to December 2017 is shown in Fig. 1, with a five-month weighted, moving average of the monthly SOI.

Fig. 2 shows the ENSO 5VAR Index over the same period, with a three-month binomially weighted moving average. The 5VAR[2] is a composite monthly ENSO index, calculated as the standardised amplitude of the first principal component of the monthly Darwin and Tahiti mean sea level pressure (MSLP) and monthly indices NINO3, NINO3.4 and NINO4 sea-surface temperatures[3] (SSTs).

Sustained negative values of the SOI below −7 typically indicate El Niño whereas sustained positive values above +7 typically indicate La Niña. Values between +7 and −7 generally indicate neutral conditions. Positive values of 5VAR that are in excess of one standard deviation are typically associated with El Niño, but negative 5VAR values below one standard deviation are indicative of La Niña.

Following a strong El Niño during 2015–2016 (Rosemond and Tobin, 2018), the ENSO remained in a neutral phase into mid-2017. From mid-2017 the tropical Pacific cooled (Martin and Tobin, 2019), and atmospheric and oceanic indicators began to consolidate in October. La Niña thresholds were reached towards the end of November. It is unusual for La Niña to develop this late in the year, but not unprecedented. For example, 2008–2009 was another recent late-starting La Niña (Mullen 2009; Qi 2009).

[1]The Troup Southern Oscillation Index (Troup, 1965) used in this article is 10 times the standardised monthly anomaly of the difference in mean sea level pressure (MSLP) between Tahiti and Darwin. The calculation is based on a 60-year climatology (1933–1992), with records commencing in 1876. The Darwin MSLP is provided by the Bureau of Meteorology, and the Tahiti MSLP is provided by Météo France inter-regional direction for French Polynesia.

[2]ENSO 5VAR was developed by the Bureau of Meteorology and is described in Kuleshov *et al.* (2009). The principal component analysis and standardisation of this ENSO index is performed over the period 1950–1999.

[3]SST indices obtained from ftp://ftp.cpc.ncep.noaa.gov/wd52dg/data/indices/sstoi.indices.

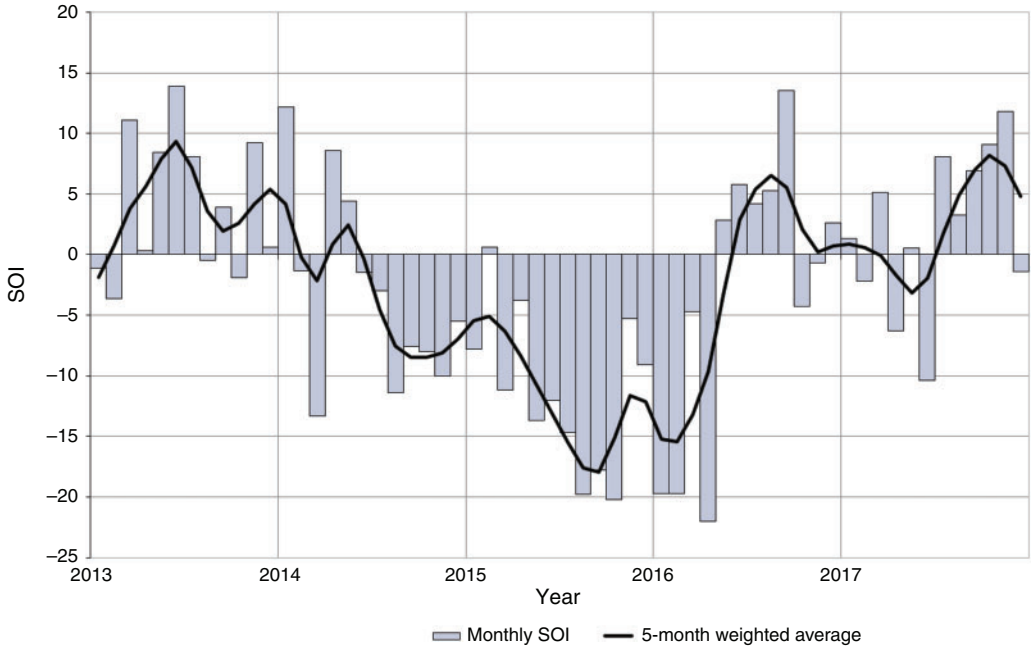

Fig. 1. Troup Southern Oscillation Index (SOI) values from January 2013 to December 2017, with a five-month binomial weighted moving average.

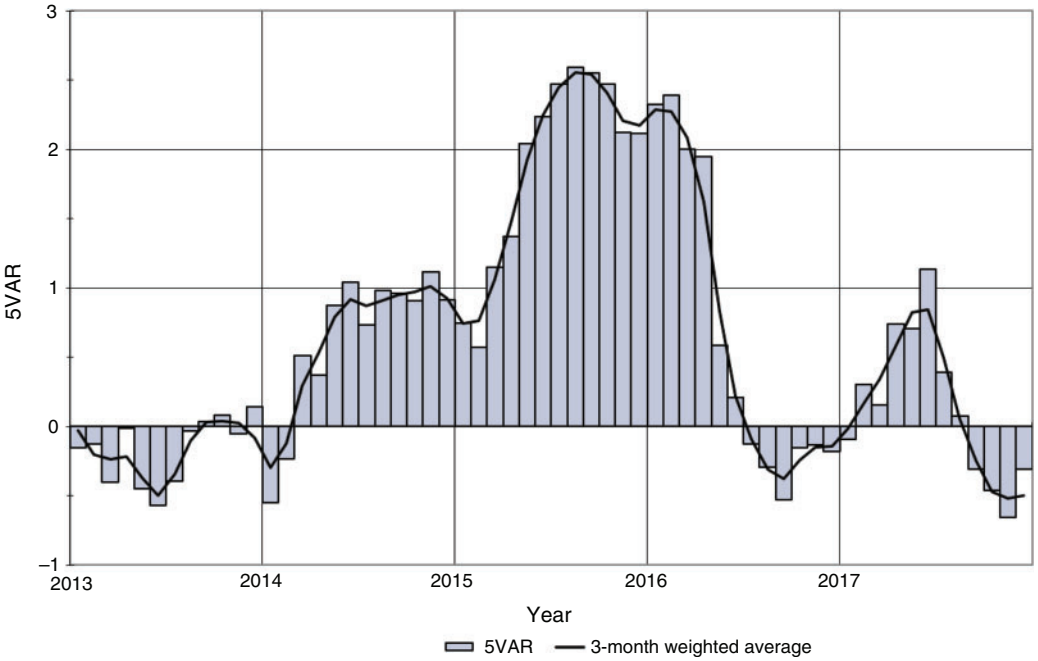

Fig. 2. Values of the composite ENSO 5VAR Index for the period January 2013 to December 2017 with the three-month binomially weighted moving average.

The SOI fluctuated within neutral bounds over the first half of 2017, before remaining above the La Niña threshold (+7) for most of the second half of the year. The spring 2017 mean value of the SOI was +9.3, with the monthly values for September, October and November being +6.9, +9.1 and +11.8 respectively.

The 5VAR index briefly rose above +1 in June 2017, having tracked a slow rise from weak negative values in the second half

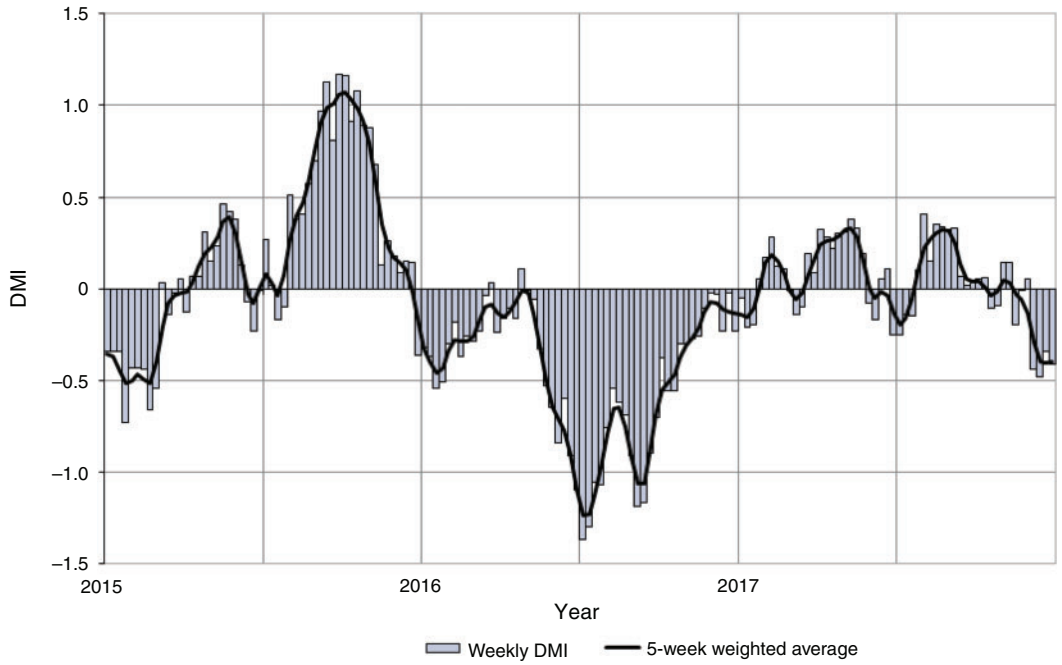

Fig. 3. Weekly Dipole Mode Index (DMI) and five-week running mean from January 2015 to December 2017.

of 2016. The rise was short-lived, however, and 5VAR values again returned to weak negative values from September through the remainder of 2017. Monthly values were –0.3 for September, –0.5 for October and −0.7 for November.

The NINO3.4 and NINO3 indices measure SSTs in the central and eastern tropical Pacific Ocean respectively, in a box covering 5°N–5°S and 120–170°W for NINO3.4, and 5°N–5°S and 150–90°W for NINO3. They are used by the Australian Bureau of Meteorology to monitor ENSO, and are closely related to the Australian climate (Wang and Hendon 2007).

The NINO3.4 values fell from weak positive values (peak value +0.49°C in June for NINO3.4, and +0.60°C in April for NINO3), with both NINO3.4 and NINO3 passing below zero early in spring 2017. The NINO3 values remained slightly stronger than NINO3.4 values throughout the season, with weekly values of NINO3 reaching the La Niña threshold (–0.8°C) first, in mid-November, before being followed by NINO3.4 at the end of November.

Mean monthly values for the season follow: –0.39°C for September, –0.36°C for October and –0.74°C for November in the case of NINO3; and correspondingly –0.25°C, –0.30°C and –0.60°C for NINO3.4[4].

The SST patterns in the eastern Indian Ocean and to the north of Australia were not typical of La Niña during the event (see Section 4), remaining near-average to slightly cooler than average in the eastern Indian Ocean (a typical event would bring warmer waters in these areas). This lack of a local warm signal to Australia's northwest partly explains the lack of a typical La Niña response in Australian rainfall.

2.2 Indian Ocean Dipole (IOD)

The IOD[5] (Saji *et al.* 1999) is the difference in SST anomalies between the western node of the tropical Indian Ocean (centred on the equator) off the coast of Somalia and the eastern node (centred south of the equator) off the coast of the Indonesian island of Sumatra. The IOD is said to be in a positive phase when values of the Dipole Mode Index (DMI) are persistently greater than +0.4°C, neutral when the DMI is persistently between –0.4°C and +0.4°C, and negative when DMI values are less than –0.4°C. Typically, to be considered a positive/negative IOD event, index values need to remain above/below the threshold for at least eight weeks.

A positive IOD often results in below average winter–spring rainfall over southern and central Australia. It also typically means warmer than average winter–spring days for the southern two-thirds of Australia. Conversely, a negative IOD is associated with an increased chance of a wetter than average winter–spring for much of the continent, with the signal strongest for the south-eastern mainland. Winter–spring temperature tends to be warmer than average in the north of Australia during negative IOD, and nights are typically cooler than average for the south-eastern mainland.

While the IOD remained neutral during 2017 (Fig. 3), a weaker positive IOD-like temperature gradient across the Indian Ocean was present for much of the year. The SSTs were higher than average in the west of the basin close to Africa, and average to below average in the eastern Indian Ocean, including around Western Australia. This temperature gradient likely contributed a weak drying influence on Australian climate as cooler surface

[4]These SST indices are calculated from the monthly NMOC SSTA analysis.

[5]http://www.bom.gov.au/climate/iod/. The western node is a box covering 10°S–10°N and 50–70°E; the eastern node is a box covering 0–10°S and 90°–110°E.

waters close to the continent limit the supply of moisture to the atmosphere, resulting in less rainfall (Section 9).

3 Tropical convection

3.1 Outgoing longwave radiation (OLR)

The OLR in the equatorial Pacific Ocean can be used as an indicator of enhanced or suppressed tropical convection. Positive OLR anomalies typify a regime of reduced convective activity, a reduction in cloudiness and, usually, rainfall. Conversely, negative OLR anomalies indicate enhanced convection, increased cloudiness and usually increased rainfall. Equatorial cloudiness near the International Date Line typically increases during El Niño (negative OLR anomalies) and decreases during La Niña (positive OLR anomalies). Similarly, when a negative IOD event is in place, OLR anomalies are negative over the eastern Indian Ocean where increased convection occurs.

The Hovmöller diagram of OLR anomalies along the equator (Fig. 4) shows a sustained period of positive OLR anomalies near the Date Line during the southern hemisphere spring 2017. Cloudiness near the Date Line had been generally below average since early August. Averaged over an area at the Date Line (7.5°S–7.5°N and 160°E–160°W), the standardised monthly OLR anomaly[6] was +0.8 for September, +0.8 for October and +1.1 for November.

Seasonal spatial patterns of OLR anomalies across the Asia–Pacific region between 40°N and 40°S for the southern hemisphere spring 2017 are shown in Fig. 5*a*, and across the globe in Fig. 5*b*. Negative OLR anomalies are evident over almost the entire Australian continent, with the strongest anomalies over central Western Australia to northwestern South Australia, consistent with above average rainfall over much of Australia for the season, particularly in inland Western Australia and western Central Australia. Negative OLR anomalies were also evident over much of the Maritime Continent to the north of Australia, and across Asia between about 10°N and 20°N. Positive anomalies are seen over the western tropical Pacific Ocean (Fig. 5*a*) and while strongest in the west, also extend across much the eastern half of the tropical Pacific on the northern side of the equator (Fig. 5*b*).

It should be noted that OLR values currently appear to have a negative bias over subtropical land areas, especially desert regions, most likely associated with orbital decay of the GOES-18 satellite (Matthew Wheeler, pers. comm.). Precipitation anomalies provide an additional means to explore variation in cloudiness. Hence, also shown (Fig. 6) is a map of the seasonal precipitation anomalies as calculated from NOAA's Climate Anomaly Monitoring System-Outgoing longwave radiation Precipitation Index (CAMS_OPI) analysis.

The OLR patterns in the Pacific are consistent with an emergent La Niña. Rainfall patterns across the broader region (see Section 9) are also consistent with an emergent La Niña with above average rainfall over Indonesia and much of the Maritime Continent, and below average rainfall over the tropical Pacific Ocean.

Precipitation during the season was below average across much of the tropical Pacific Ocean, the northern half of South America and Mesoamerica, and to a lesser degree for large parts of south-eastern Australia, the Tasman Sea and New Zealand. Precipitation was above average across the far western Pacific Ocean and the Maritime Continent, much of the northeast of the Indian Ocean, eastern areas of the Caribbean Sea and the Sargasso Sea.

3.2 Madden-Julian Oscillation (MJO)

The MJO is a tropical convective wave anomaly which develops in the Indian Ocean and propagates eastwards into the Pacific Ocean (Madden and Julian 1971, 1972, 1994). The MJO takes approximately 30–60 days to reach the western Pacific, with a frequency of 6–12 events per year (Donald *et al.* 2004). When the MJO is in an active phase, it is associated with areas of increased and decreased tropical convection, with effects on the southern hemisphere often weakening during early autumn, before transitioning to the northern hemisphere. A description of the Real-time Multivariate MJO (RMM) index and the associated phases can be found in Wheeler and Hendon (2004).

The phase-space diagram of the RMM for spring 2017 is shown in Fig. 7. While weak during September and nearly all of November, the MJO was strong for much of October. An active pulse of convection passed through the Maritime Continent during mid-October, and moved through the western Pacific Ocean during the second half of the month. The MJO is associated with strengthened easterly wind anomalies in the Pacific while it is active over the Maritime Continent; but when over the western Pacific Ocean, it is likely to see somewhat decreased trade wind strength.

The passage of the MJO is illustrated by the eastward progression of positive wind anomalies (pink shading) during October in Fig. 8. This activity likely contributed to a strengthening of the trade winds over the tropical Pacific during October, which was in turn associated with a temporary halt in the cooling of SSTs and a pause in La Niña development. This activity may have also contributed to above average rainfall over Queensland during October (see Section 8), as the MJO is associated with above average rainfall over eastern Australia, particularly the tropics, in phases 5–7 during spring.

4 Oceanic patterns

4.1 Sea surface temperatures (SSTs)

Fig. 9 shows SST anomalies globally for spring 2017, relative to 1961–1990. Fig. 10 shows SST deciles, based on the full period of historical observations since 1900.

The SSTs were warmer than average across much of the world's oceans, particularly across the northern hemisphere. For the globe as a whole, monthly SSTs were the warmest on record for September (+0.64°C), equal-warmest on record for October (+0.61°C) and third warmest on record for November (+0.53°C)[7].

[6]Standardised monthly OLR anomalies obtained from https://www.cpc.ncep.noaa.gov/data/indices/olr.

[7]Values compared to the 1961–1990 average, using ERSST v5 data.

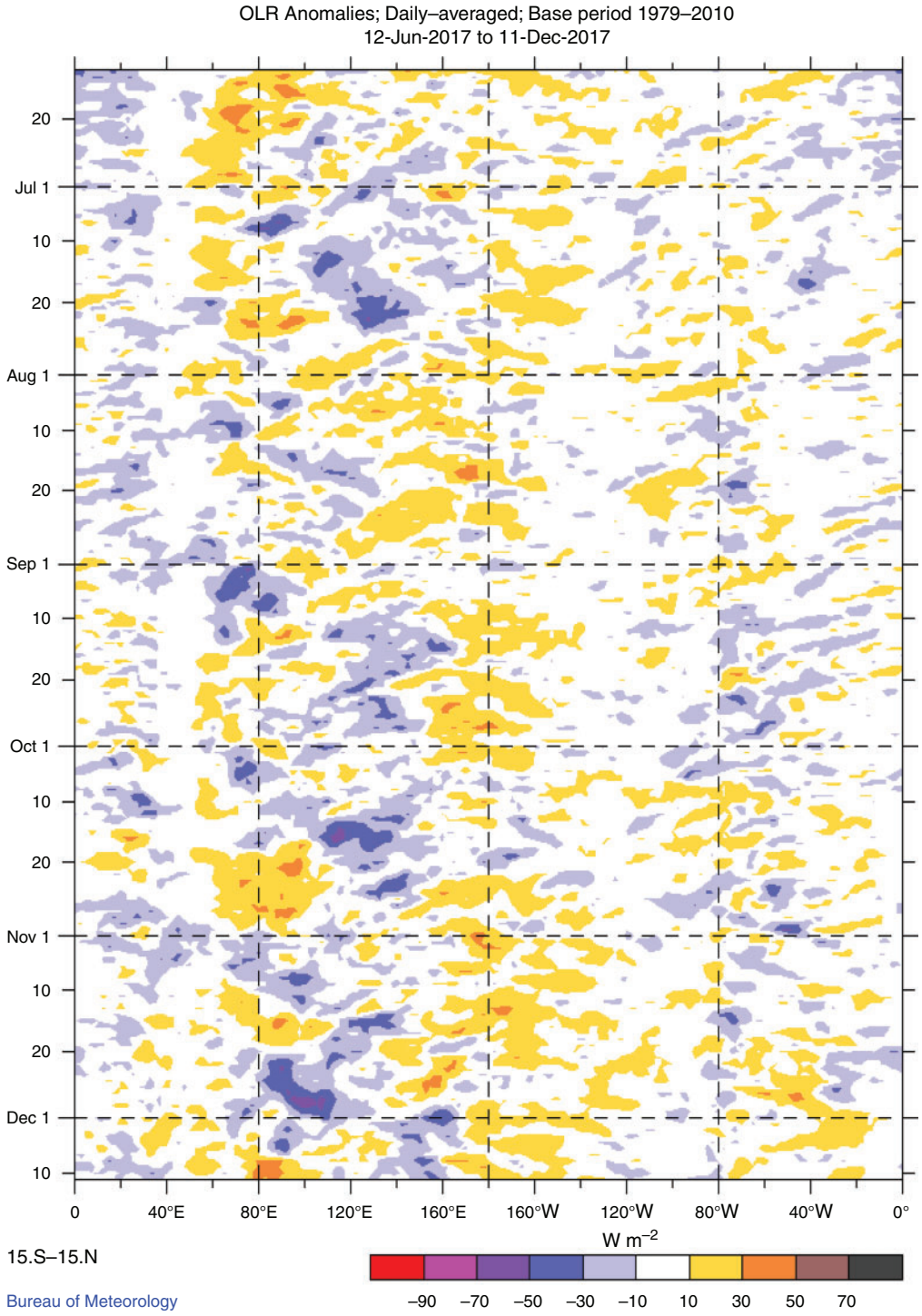

Fig. 4. Time-longitude plot of daily-averaged outgoing longwave radiation (OLR) anomalies, averaged over 15°S–15°N, for the period 12 June to 11 December 2017. The OLR anomaly is from daily data with respect to a base period of 1979–2010, using interpolated OLR data provided by the NOAA/OAR/ESRL PSD, Boulder, Colorado, USA.

For the Australian region anomalies were less strong, with September ninth-warmest on record (+0.48°C), October equal-sixth-warmest (+0.54°C) and November third-warmest (+0.67°C). For spring as a whole, SSTs were fifth-warmest on record for the Australian region (+0.56°C).

The SSTs were within half a degree of average temperatures across much of the southern hemisphere, with anomalies of half to one degree warmer than the 1961–1990 average over most of western and northern Indian Ocean, the Maritime Continent and waters around northern Australia, from the east of the Great

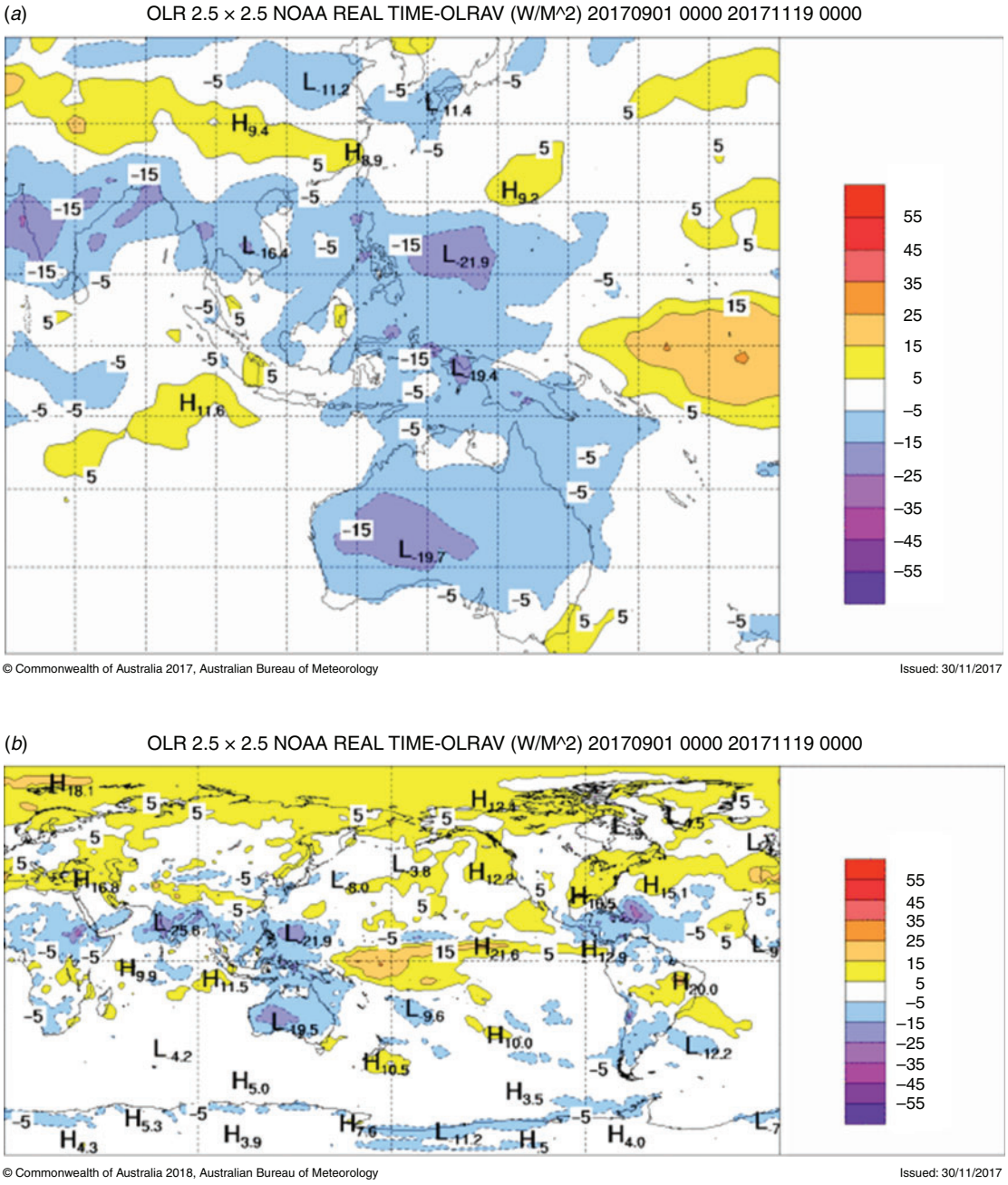

Fig. 5. The OLR anomalies for the period from 1 September to 19 November 2017 (W m^{-2}). Anomalies calculated with respect to base period 1979–2000. The upper panel (*a*) shows the region between 40°N and 40°S and 70°E and 180°E, while the lower panel (*b*) shows the entire globe.

Australian Bight and across most of the western half of the southern Pacific Ocean, and in an area of the southwestern South Atlantic Ocean south of 30°S.

The tongue of weak cool anomalies up to one degree cooler than average extending along the equator in the central to eastern Pacific is consistent with the emergence of La Niña during the course of the season.

In the Australian region, anomalies exceeded one degree in parts of the Tasman Sea, and in waters close to the shores of the Gulf of Carpentaria, the western Top End and the Kimberley. The decile map shows SSTs were very much above average around most of Australia, and warmest on record for part of the Tasman Sea, but near-average around the southwest of Australia.

4.2 Equatorial subsurface patterns

The 20°C isotherm depth is generally located close to the equatorial thermocline, which is the region of greatest temperature gradient with depth and is the boundary between the warm

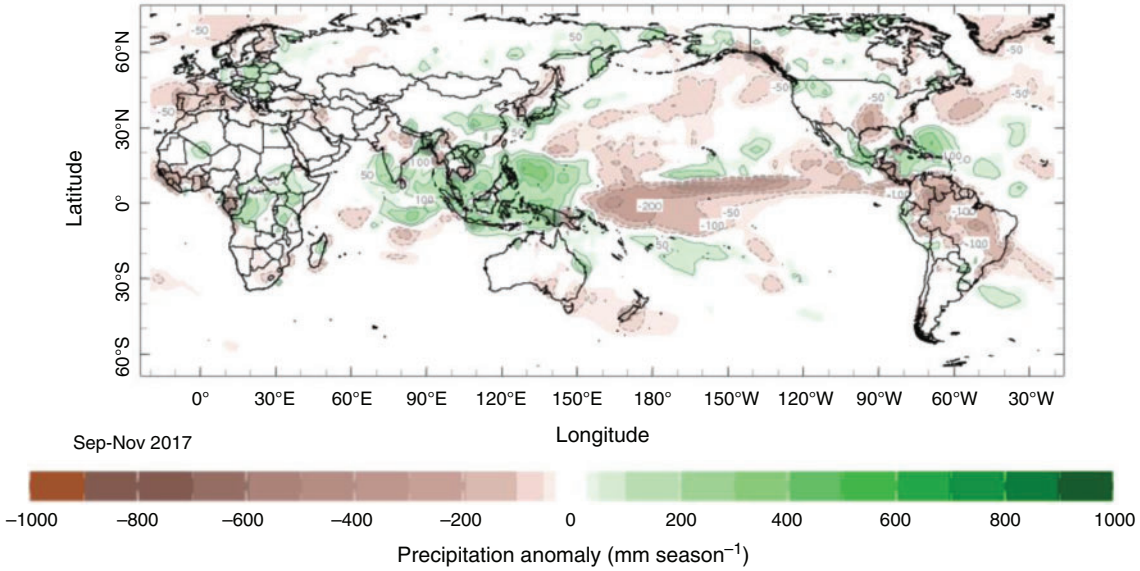

Fig. 6. Global precipitation anomalies for spring 2017 (mm season^{-1}) from NOAA CAMS_OPI. Base period is 1979–2000.

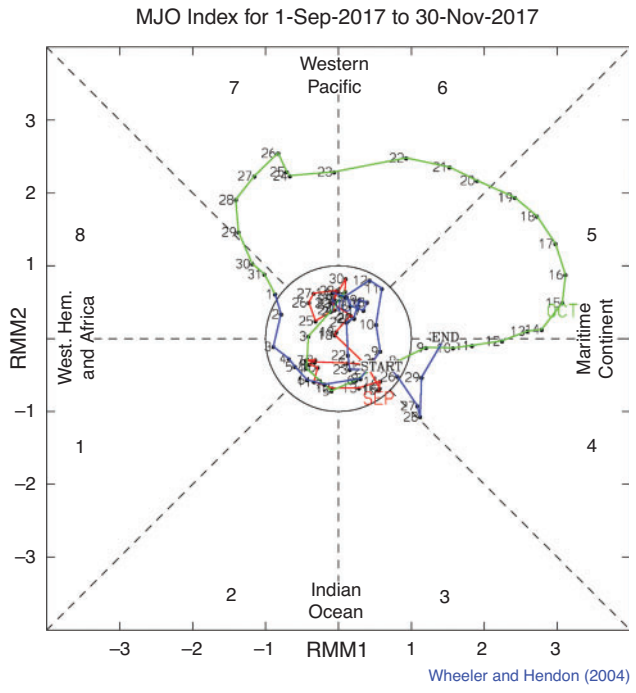

Fig. 7. Real-time Multivariate MJO (RMM) phase-space diagram for 1 September to 30 November 2017. Daily values are shown with September in red, October in green and November in blue. The eight phases of the MJO and the corresponding (approximate) locations of the near-equatorial enhanced convective signal are labelled.

near-surface and cold deep-ocean waters. Therefore, measurements of the 20°C isotherm depth make a good proxy for the thermocline depth. Negative anomalies correspond to the 20°C isotherm being shallower than average and indicates cooling of subsurface temperatures. If the thermocline anomaly is positive, the depth of the thermocline is deeper. A deeper thermocline results in less cold water available for upwelling, and therefore a warming of subsurface temperatures.

Subsurface waters were generally cooler than average in the equatorial Pacific during the southern hemisphere spring 2017 (Fig. 12), although weak warm anomalies developed in the shallow subsurface of the far western equatorial Pacific as the season progressed. Correspondingly, the thermocline was generally shallower than usual (Fig. 11) in the central to eastern equatorial Pacific, and generally near-average depth in the west with small positive anomalies (shallower thermocline) near the Date Line towards the end of the season.

Subsurface temperature anomalies remained fairly similar across the three months September, October and November, aside from the slight warming in the west. Small areas of central or eastern equatorial Pacific subsurface reached up to 4 degrees cooler than average in each of the three months. Cool subsurface anomalies did go on to strengthen further in December 2017, but the moderate strength of the subsurface anomalies shown here is representative of the fairly weak nature of the 2017–2018 La Niña.

5 Sea ice

Antarctic sea ice usually reaches its annual maximum extent in mid- to late September. The annual maximum Antarctic sea ice extent[8] was close to record-low during spring 2017, and reached

[8]Sea ice information is sourced from the National Snow and Ice Data Center (https://nsidc.org/arcticseaicenews/charctic-interactive-sea-ice-graph/).

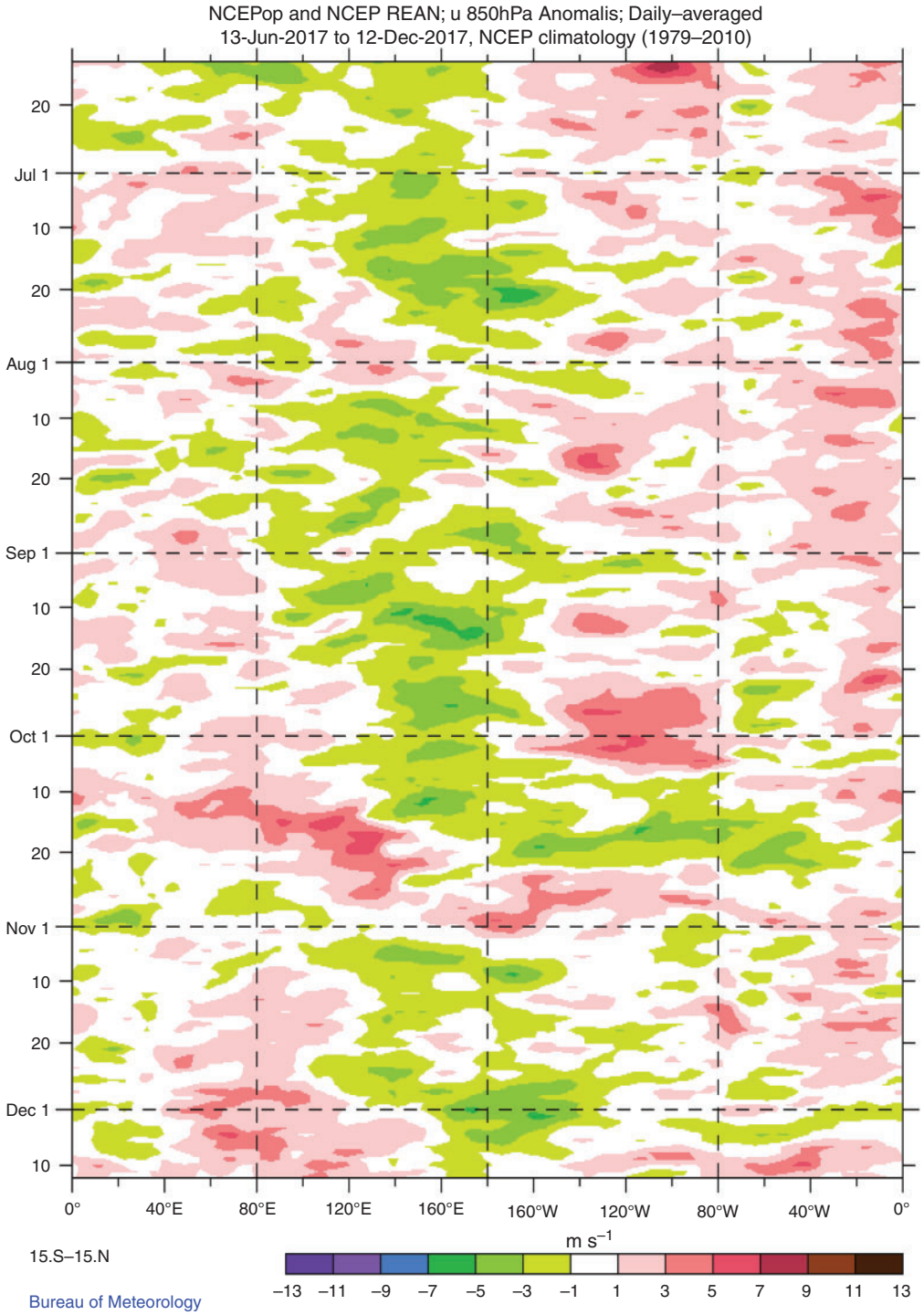

Fig. 8. Time-longitude plot of westerly wind anomalies, averaged over 15°S to 15°N, for the period 13 June to 12 December 2017. The OLR anomaly is from daily data with respect to a base period of 1979–2010, using interpolated OLR data provided by the NOAA/OAR/ESRL PSD, Boulder, CO, USA.

a peak later than usual at 18.10 million km^2 during 10–12 October (about 0.05 million km^2 above values achieved in mid-September 2017). Only 1986 had lower maximum daily extent during the winter–spring period, and 2002 had a similar winter–spring sea ice extent to 2017.

The mean September, October and November extents, 17.90, 17.81 and 15.39 million km^2 respectively, were 0.57, 0.35 and 0.76 million km^2 below their corresponding 1981–2010 medians. The northern edge of the sea ice during October was north of its mean climatological position (i.e. more ice than average) between

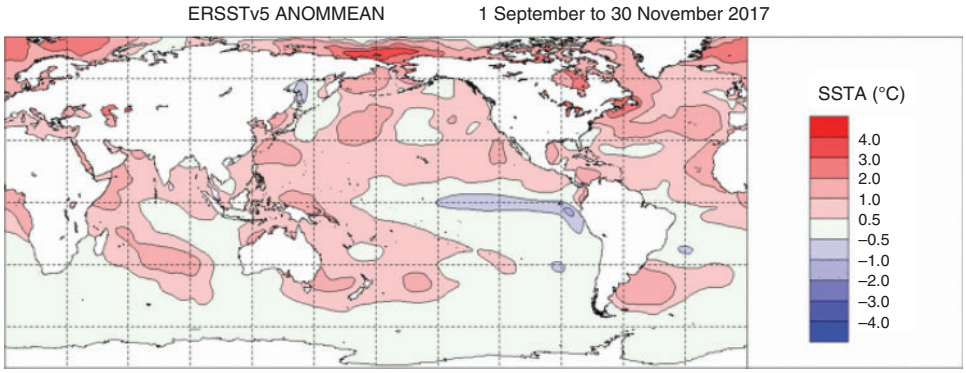

Fig. 9. Global sea-surface temperature anomaly (SSTA,°C) from 1961–1990 averages for austral spring 2017 (Extended Reconstructed Sea-Surface Temperature Version 5, ERSSTv5; Huang *et al.* 2017).

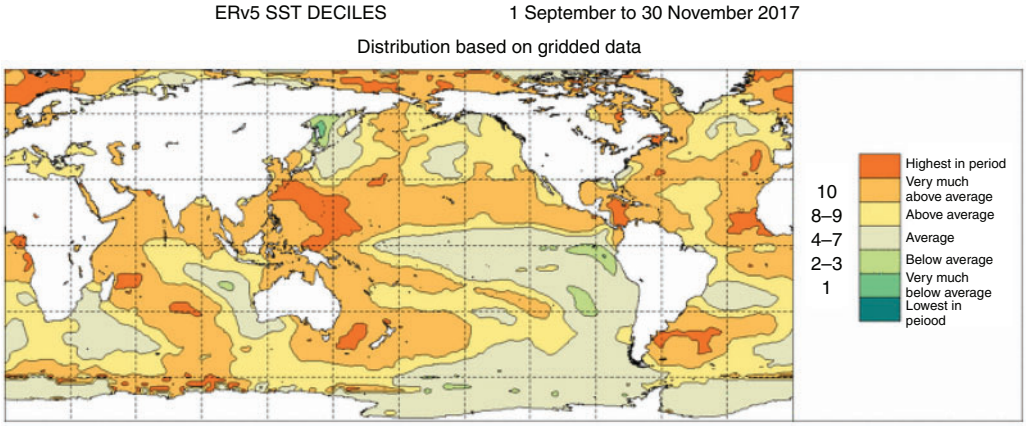

Fig. 10. Global sea-surface temperature (ERSSTv5) decile map for spring 2017, compared to observations since 1900.

about 135°W and 60°W, in a small area around 30°E and between 120°E and 135°E; conversely there was less ice than average (i.e. south of its climatological mean) between 60°W and around 150°E, between 60°E and 120°E, and between 180°W and 135°W.

The lowest minimum Antarctic sea ice extent on record was observed in early March 2017, with monthly extents remaining among the lowest on record low throughout the year. The satellite record begins in 1979.

6 Atmospheric circulation

6.1 Southern Annular Mode (SAM)

The SAM commenced spring 2019 in a strongly positive phase, with index values above +2 from late August[9] (Fig. 13). Values dropped to near zero in the middle of September before again rising above +2 late in the month. Values were moderately negative throughout the second half of October and early November, dropping to below +1 for part of the second half of October and again in early November, before briefly rising to above +1 just before mid-November, and remaining near or above +2 for the last third of November. Monthly mean values of the Climate Prediction Center (CPC) SAM index were +1.29 for September, –0.57 for October, and −0.77 for November.

Positive values of the SAM index during spring and early summer are associated with increased onshore flow in parts of eastern Australia, which typically increases the likelihood of above average rainfall in much of New South Wales and parts of southern Australia, and below average rainfall in western Tasmania (Hendon *et al.* 2007). Conversely, negative SAM has roughly the inverse effect. The SAM also has an impact on temperatures. In general, in areas where rainfall is increased, temperature is decreased but where rainfall is decreased, temperature is increased.

It is possible that the positive phase of SAM during the second half of September contributed to widespread warmth and early season temperature records in eastern Australia. The SAM was also positive in late November to early December, likely contributing to the rainfall event in south-eastern Australia at the start of December. See Section 8 for further detail on both of these events.

[9]For more information on the SAM index from the NOAA Climate Prediction Center (CPC), see http://www.cpc.ncep.noaa.gov/products/precip/CWlink/daily_ao_index/aao/aao.shtml.

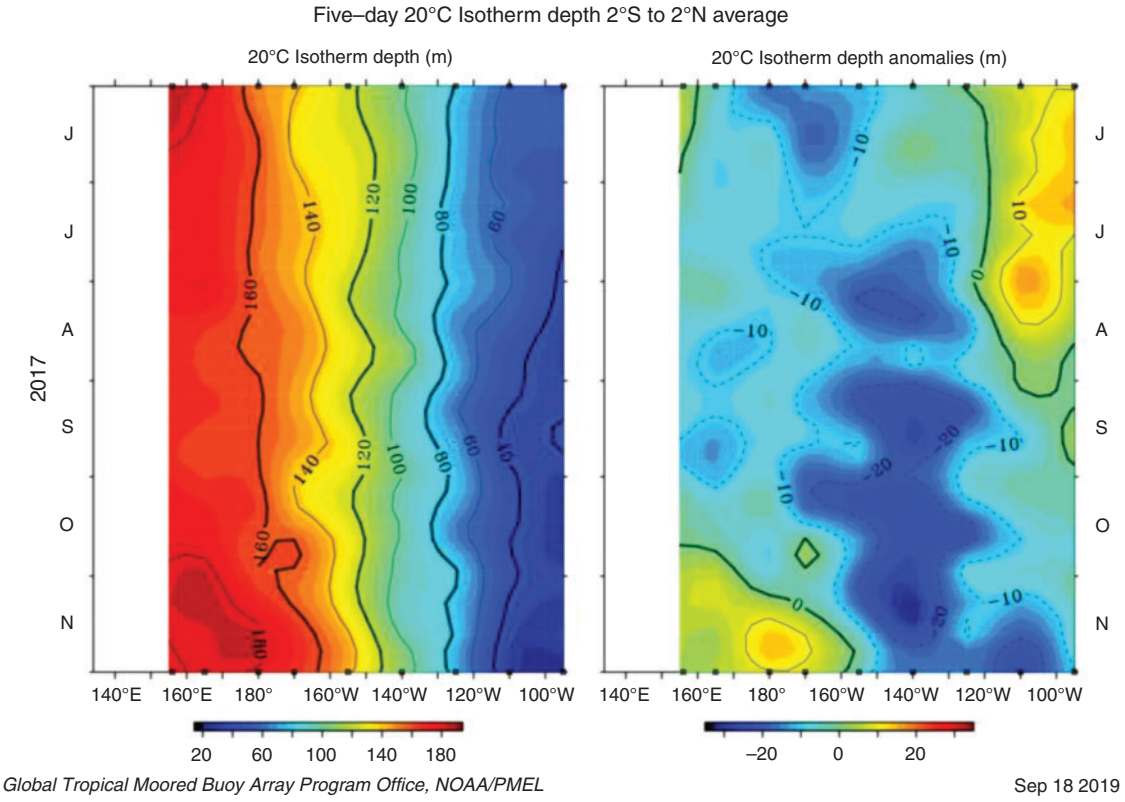

Fig. 11. Hovmöller diagram of the 20°C isotherm depth and anomaly along the equator for June–November 2017, obtained from NOAA's TAO/TRITON data (https://www.pmel.noaa.gov/tao/drupal/disdel/).

6.2 Surface analyses

The MSLP pattern for spring 2017 is shown in Fig. 14, computed using data from the 0000 UTC daily analyses of the Bureau of Meteorology's Australian Community Climate and Earth System Simulator (ACCESS) model[10]. The MSLP anomalies are shown in Fig. 15, relative to the 1979–2000 climatology obtained from the National Center for Environmental Prediction (NCEP) II Reanalysis data (Kanamitsu *et al.* 2002). The MSLP anomaly field is not shown over areas of elevated topography (grey shading).

The seasonal MSLP analysis chart for spring 2017 (Fig. 14) was distinctly zonal in the southern hemisphere mid- to high-latitudes. The subtropical ridge was evident across the mid-latitudes, including southern Australia. Centres of high pressure were observed over the southern Indian Ocean (reaching 1022.5 hPa at 90°E 30°S), the South Atlantic (reaching 1025.0 hPa at 15°E 30°S) and the eastern South Pacific (reaching 1025.2 hPa at 90°W 30°S).

The MSLP was close to average over most of the southern hemisphere (Fig. 15), with areas of weak positive anomalies present in the South Pacific, reaching +3.63 hPa at about 150°W 40°S, and across a broader area of the South Atlantic between about 50°S and 20°S and 0° and 40°W and approaching the coast of Peru.

The belt of low pressure close to the Antarctic coast was also stronger than average across the peninsula region from the Amundsen Sea to the Weddell Sea, with anomalies reaching –5.00 hPa over much of this region. This is consistent with SAM having been positive for much of the season. The polar low shows a minimum pressure of 973.2 hPa on the coast of West Antarctica around 120°W.

6.3 Mid-tropospheric analyses

The 500 hPa geopotential height, an indicator of the steering of surface synoptic systems across the southern hemisphere, is shown for spring 2017 in Fig. 16. The associated anomalies are shown in Fig. 17.

Geopotential height is valuable for identifying and locating features such as troughs and ridges which are the upper-level equivalents of surface low and high pressure systems respectively. Coinciding with the surface features discussed above, an anomalous trough is evident along the west coast of the Antarctic Peninsula. Generally, pressure anomalies were close to average across the southern hemisphere, though there was weak anomalous ridging over the South Atlantic Ocean extending from the coast of Peru to East Antarctica between about 0°E and 30°E, and also extending over the Polar Plateau.

[10]For more information on the Bureau of Meteorology's ACCESS model, see http://www.bom.gov.au/nwp/doc/access/NWPData.shtml.

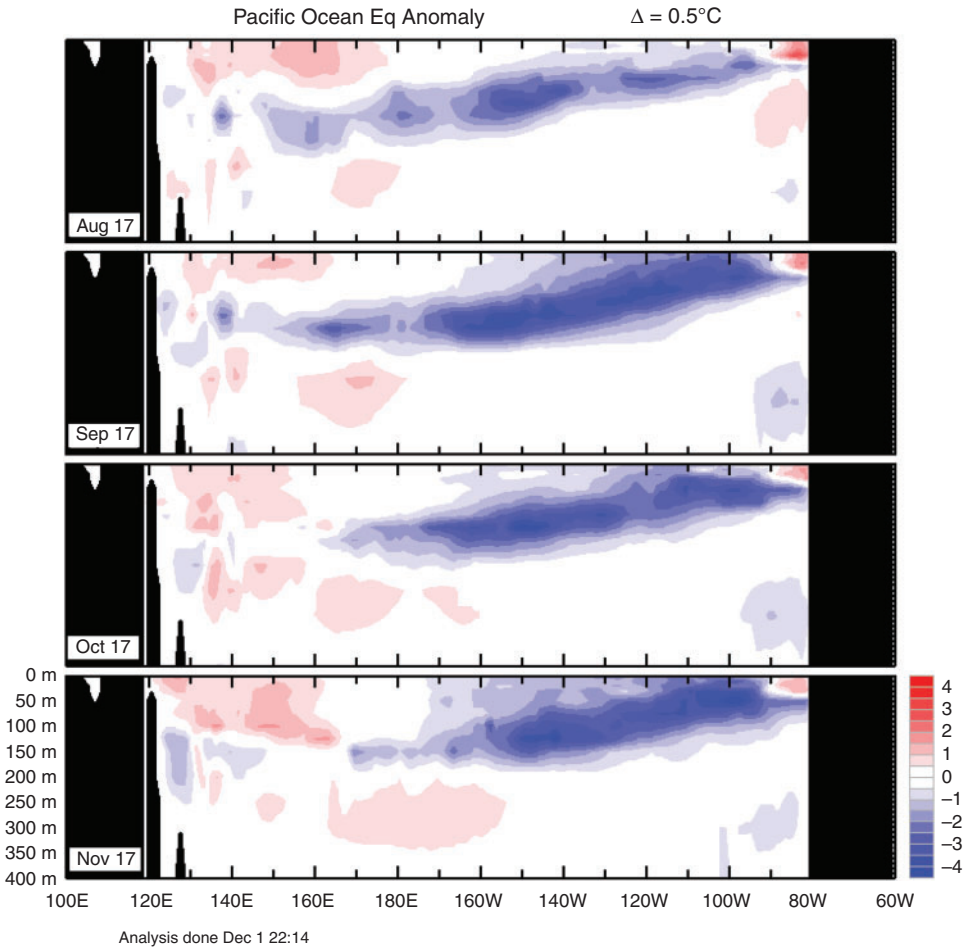

Fig. 12. The cross-section of monthly equatorial subsurface temperature anomalies for August–November 2017. Red shading indicates positive (warm) anomalies, and blue shading indicates negative (cool) anomalies.

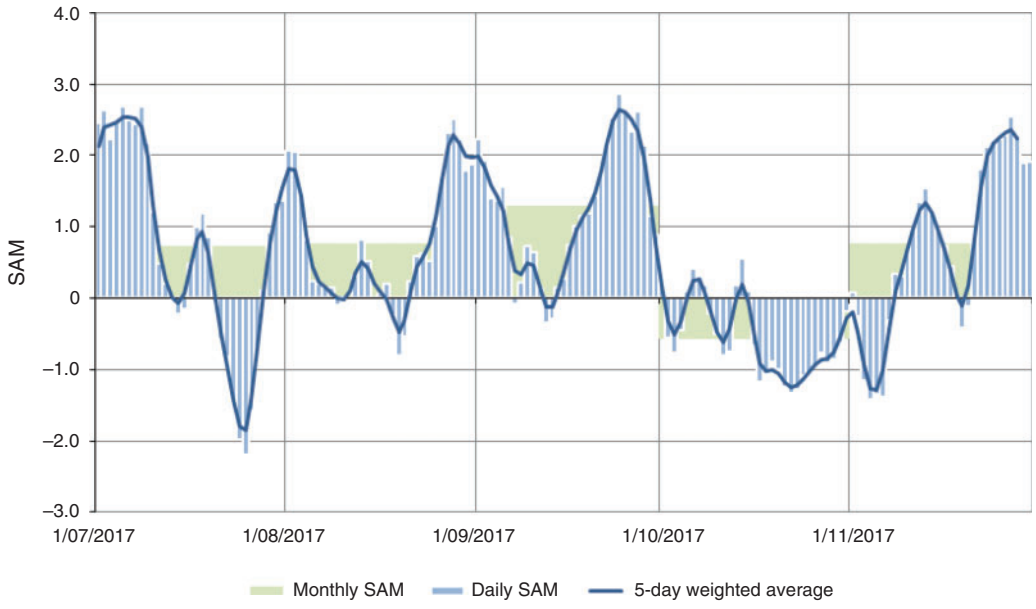

Fig. 13. Standardised AAO (SAM) index for July–November 2017. Each daily value has been standardised by the standard deviation of the monthly AAO index from 1979–2000.

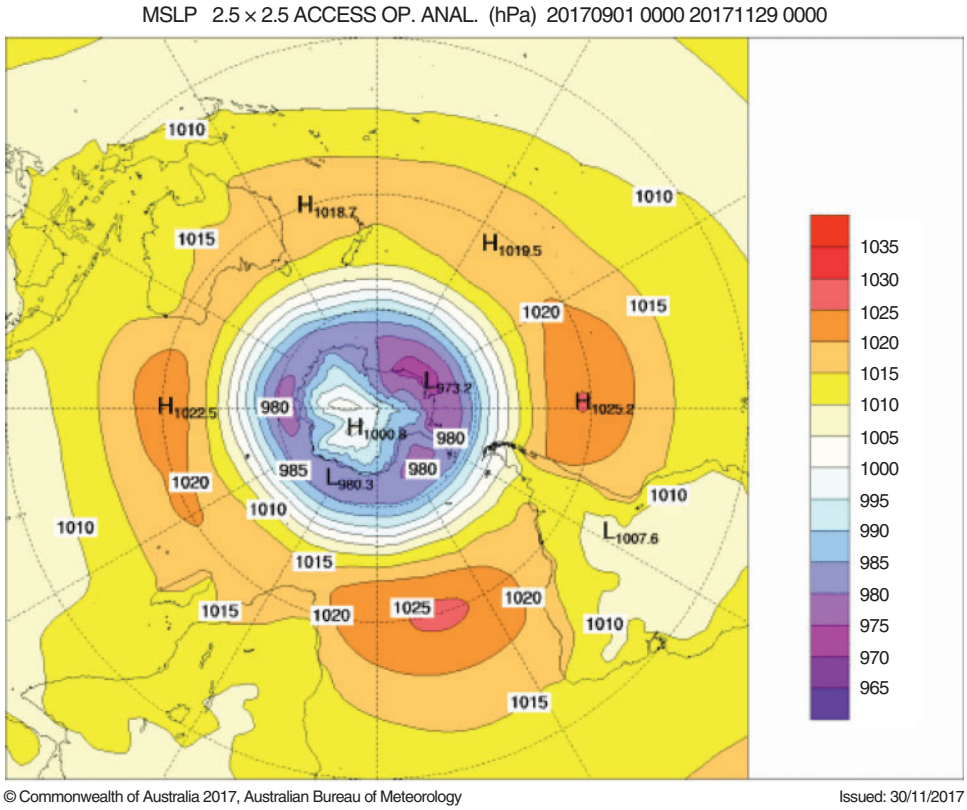

Fig. 14. Southern hemisphere mean sea-level pressure (MSLP) pattern for spring 2017.

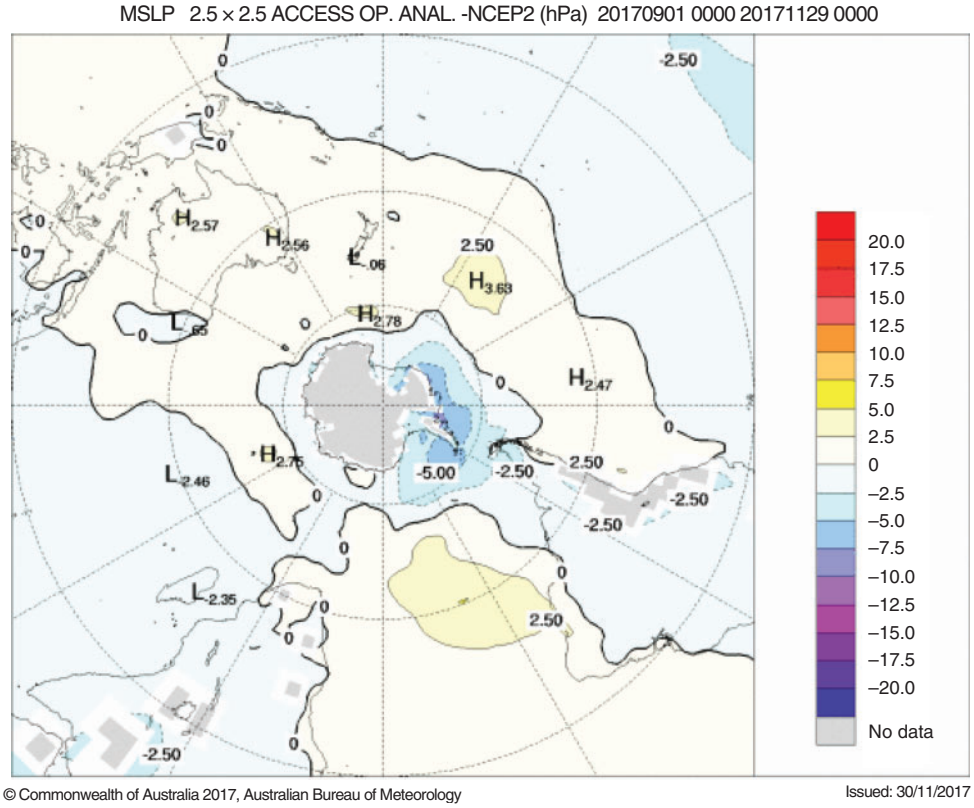

Fig. 15. Southern hemisphere mean sea-level pressure (MSLP) anomalies (hPa) for spring 2017. Anomalies calculated with respect to base period of 1979–2000.

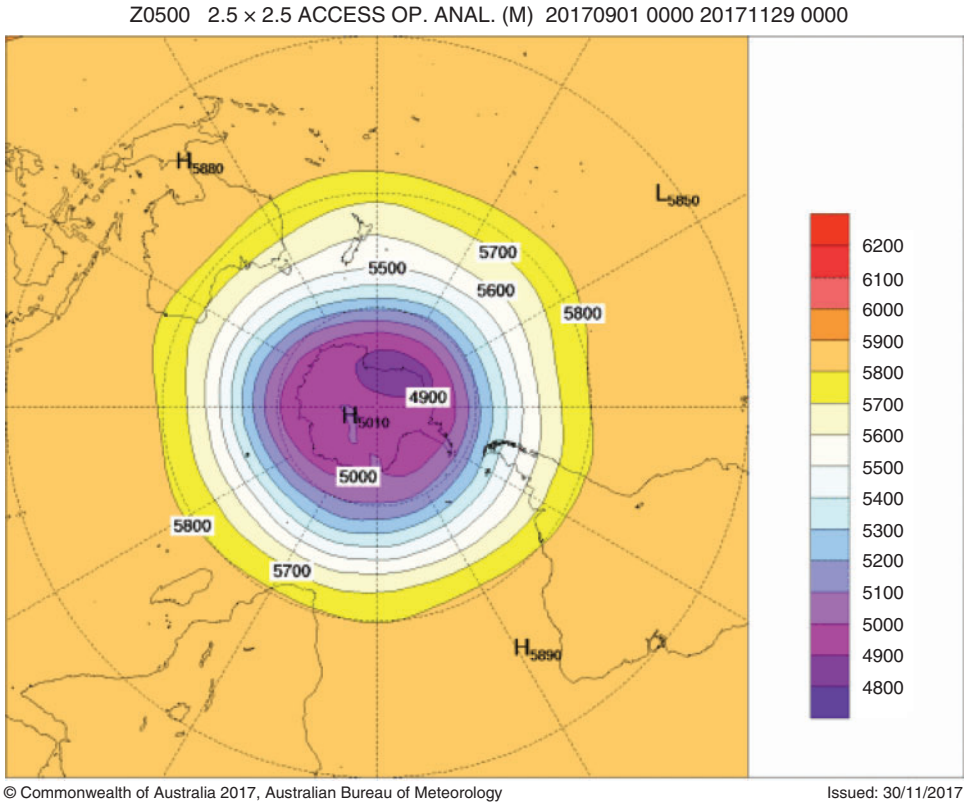

Fig. 16. Spring 2017 500 hPa mean geopotential height (gpm).

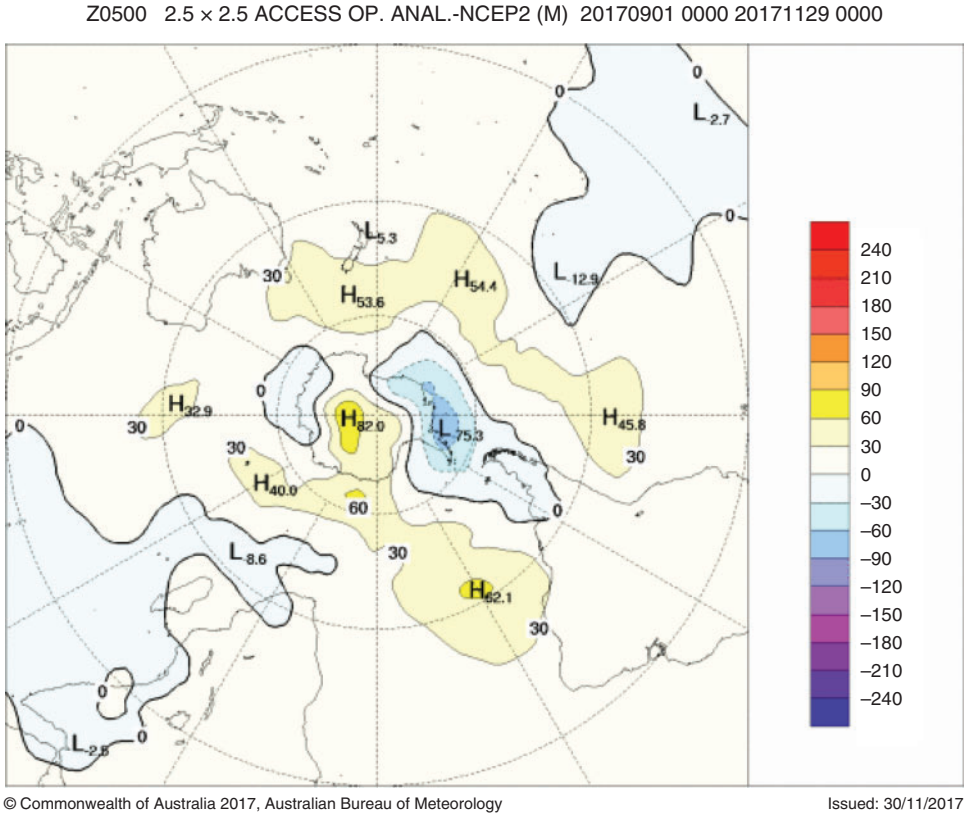

Fig. 17. The 500 hPa mean geopotential height anomalies (gpm) for spring 2017, relative to 1979–2000.

7 Winds

Figs 18 and 19 show spring 2017 low-level (850 hPa) and upper-level (200 hPa) wind anomalies respectively. Winds are computed from ACCESS and anomalies with respect to the 22-year 1979–2000 NCEP climatology. Isotach contours are at an interval of 5 m s^{-1}.

The 850 hPa winds were generally close to average in the Australian region, and were also close to average over the broader southern hemisphere. The strongest 850 hPa wind anomalies were in an area where winds were converging over Antarctic between 180°W and 90°W, on the southern side of the anomalous surface trough noted in Section 6.

At the 200 hPa level, wind anomalies were generally close to average or very weak. Areas of weak westerly wind anomalies were present in the southern hemisphere mid-latitudes, associated with an anticyclonic pattern in the southern Indian Ocean, and from the southeast Pacific across South America into the South Atlantic associated with an anticyclonic pattern to the east of South America. Westerly wind anomalies of just below 10 m s^{-1} also extended across the eastern half of the equatorial Pacific Ocean. These upper-level westerly anomalies may have been associated with the initial stages of strengthening of the Walker Circulation as La Niña developed towards the end of spring.

8 Australian region

8.1 Rainfall

Rainfall for spring 2017 was above average nationally, but mixed over individual months and across Australia geographically. Averaged nationally[11], it was the 26th-wettest spring in

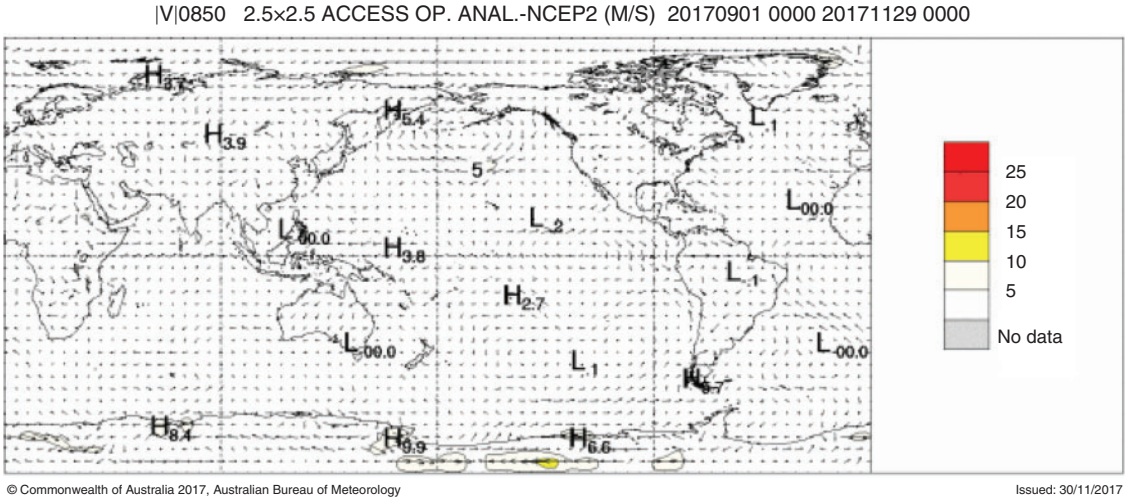

Fig. 18. The 850 hPa vector wind anomalies (m s^{-1}) for spring 2017.

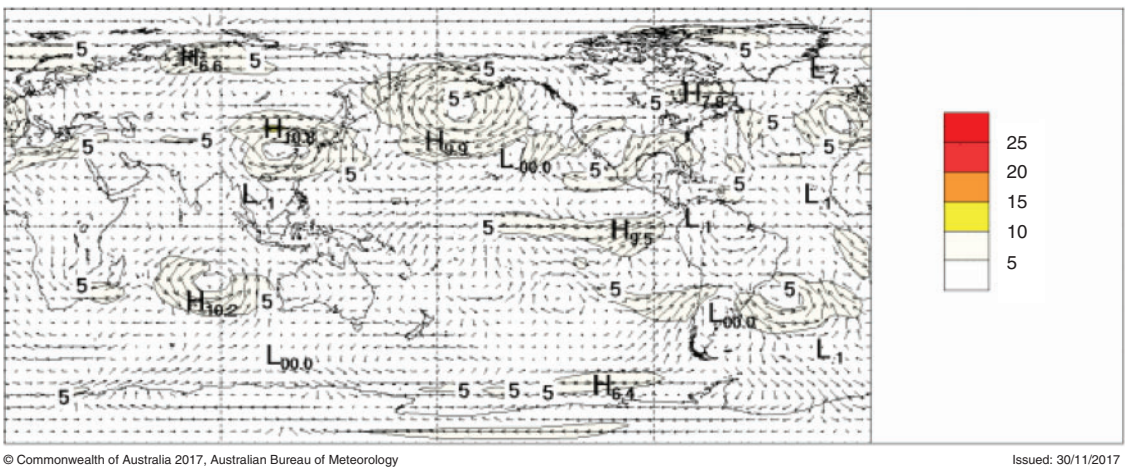

Fig. 19. The 200 hPa vector wind anomalies (m s^{-1}) for spring 2017.

[11]Rainfall reported in this section is based on the Australian Water Availability Project (AWAP) dataset (Jones *et al.* 2009).

118 years of record, with seasonal rainfall 26% above the 1961–1990 average (Table 1). Rainfall for the season (Fig. 20*a*) was above average for much of the Northern Territory, the north-western half of South Australia, large areas of northern and eastern Queensland, and large areas of Western Australia covering the Gascoyne, Interior and Kimberley. The season was drier than average for much of Tasmania, particularly in the east, the eastern half of Victoria, parts of eastern New South Wales and parts of South Australia between the northern Eyre Peninsula and the Fleurieu Peninsula.

September rainfall was particularly low over New South Wales, northern Victoria, central southern and south-eastern South Australia, and the south-eastern quarter of Queensland. It was the driest September on record for the Murray–Darling Basin as a whole. Conversely, October was exceptionally wet for Queensland, coming in as the third-wettest on record for that month. October saw high rainfall over most of Queensland and New South Wales, as well as for the Kimberley and the Interior of Western Australia, and the coast of the eastern half of the Top End in the Northern Territory.

It was the wettest October on record for parts of the Wide Bay, Burnett and North Tropical Coast districts in Queensland with several heavy rainfall events during the month, resulting in flooding in some regions, particularly around Bundaberg from mid-October. Above average October rainfall in southeast Queensland was primarily driven by enhanced easterly flow across warm ocean waters to the east of Australia (associated with a strong pulse of the MJO over the Maritime Continent), a mid-level trough situated along the northern and central Queensland coastline and a region of high pressure over the Tasman Sea.

September rainfall was also above average for the western half of Western Australia, particularly the Gascoyne and the southern Pilbara, for northern South Australia and the adjacent southern border regions of the Northern Territory, and for south coast Victoria and western Tasmania.

November rainfall was closer to average overall, but very much below average for Tasmania and Gippsland in Victoria, but above average for the Northern Territory, South Australia, eastern border regions of Western Australia and much of western Victoria.

8.2 Rainfall deficiencies

May, June and July 2017 were particularly dry across southern Australia, with August also drier than average across the northern half of New South Wales. This resulted in the emergence of serious or severe rainfall deficiencies (rainfall below the 10th or fifth percentile respectively) for the periods commencing March and June 2017. Rainfall deficiencies were evident across large areas along the west coast and northwest of Western Australia, parts of southern pastoral South Australia, large areas of New South Wales, parts of Gippsland in Victoria, eastern Tasmania and parts of Queensland in both the west and east of the state at different timescales (Fig. 21*a* and *b*).

September rainfall was very much below average over New South Wales, northern Victoria and large parts of Queensland and South Australia, initially seeing the severity and extent of rainfall deficiencies increase. However, above average rainfall in New South Wales and Queensland for October, and in South Australia and parts of western Victoria and southern New South Wales for November, significantly reduced deficiencies accumulated over the preceding 6–9 months. By the end of spring 2017, deficiencies remained at

Table 1. Summary of the seasonal rainfall ranks and extremes on a national and state basis for spring 2017. The rank refers to 1 (lowest) to 118 (highest) and is calculated over the years 1900–2017 inclusive

Region	Highest seasonal total (mm)	Highest daily total (mm)	Area-averaged total (mm)	Rank of area-averaged total	Difference from mean (%)
Australia	1370.8 mm at Bellenden Ker Top Station (Qld)	389.0 at Makowata (Qld) on 18 October	91.4	93	+26
Queensland	1370.8 mm at Bellenden Ker Top Station	389.0 at Makowata on 18 October	121.0	98	+44
New South Wales	516.9 at Doon Doon (McCabes Road)	133.0 at Brushgrove (Clarence Street) on 15 October	109.9	57	–11
Victoria	618.6 at Falls Creek (Rocky Valley)	80.4 at Canary Island on 16 November	150.4	39	–17
Tasmania	926.2 at Mount Read	51.6 at Scotts Peak Dam on 27 November	312.3	36	–14
South Australia	263.4 at Crafers (Mt Lofty)	81.0 at Mintabie on 30 September	77.7	105	+53
Western Australia	346.5 at Walpole	88.4 at Mount William on 21 September	55.5	96	+35
Northern Territory	621.2 at Pirlangimpi Airport	120.2 at Snowdrop Creek on 27 November	98.7	99	+46

(*a*)

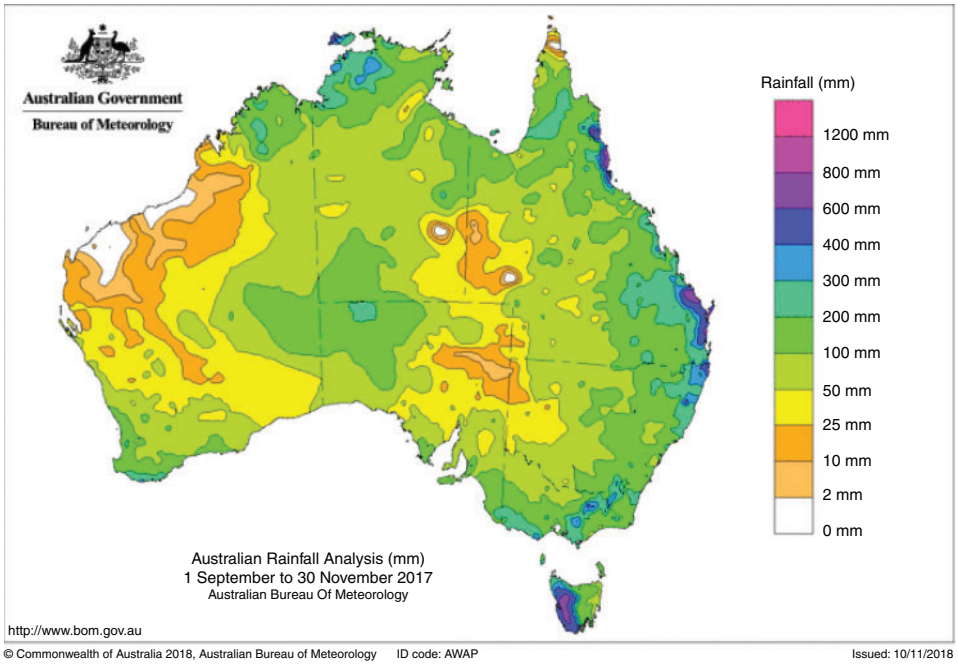

(*b*)

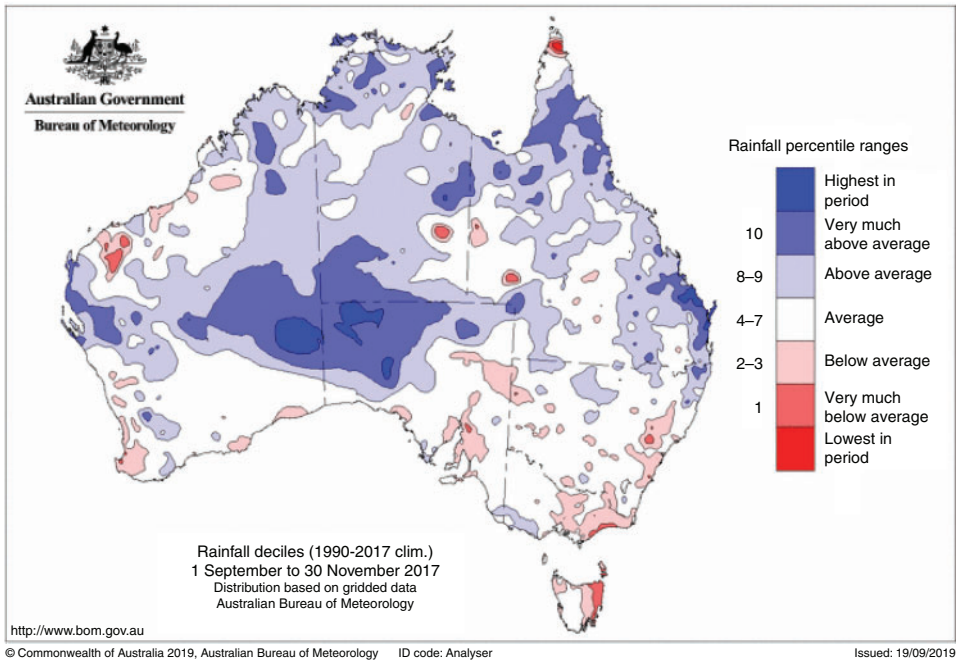

Fig. 20. (*a*) Rainfall totals and (*b*) rainfall deciles for spring 2017; decile ranges based on grid-point data with respect to all available data 1900–2017.

both timescales in parts of coastal South Australia near Ceduna and Port Augusta, across much of Gippsland in Victoria and in eastern Tasmania. For the period commencing June 2017, rainfall deficiencies also remained in New South Wales in areas between the west of the state and the Central Tablelands and western slopes of the Great Dividing Range.

In Western Australia, rainfall deficiencies also decreased during spring, with above average rain in much of the west in

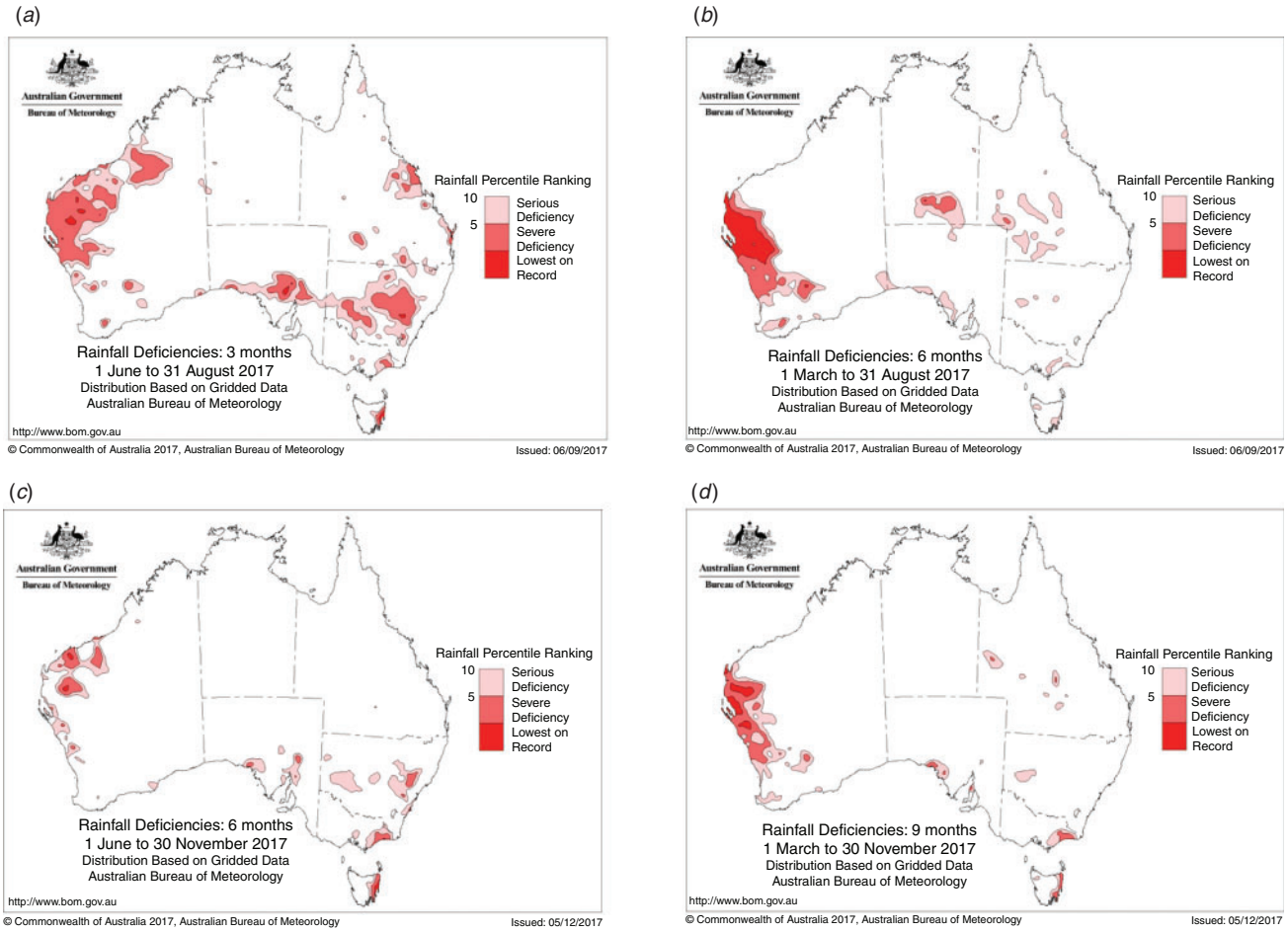

Fig. 21. Rainfall deficiencies at the start of spring for: (*a*) the 3-month period June–August 2017, (*b*) the 6-month period March–August 2017; and at the end of spring for (*c*) the 6-month period June–November 2017 and (*d*) the 9-month period March–November 2017.

September, the north and east in October and over scattered parts in November. At the end of spring deficiencies persisted in areas along the coast of Western Australia in the Gascoyne and Pilbara for the period commencing June 2017, and along the west coast of Western Australia between about Exmouth and Perth as well as pockets of the southwest and the Goldfields district for the period commencing March 2017.

For the three-month season of spring 2017 itself, rainfall was below the 10th percentile for east coast Tasmania, the Gippsland coast in Victoria and a small pocket at the tip of Cape York Peninsula in Queensland (Fig. 20*b*). Rainfall for spring was in decile 1 for 15.4% of Tasmania (Table 2).

8.3 Temperature

Spring 2017 was exceptionally warm for Australia. All regions except the Northern Territory observed mean temperatures for the season among the 10 warmest on record, and for Australia as a whole it was the equal-fifth-warmest spring on record. Both maximum and minimum temperatures were above to very much above average over the majority of Australia. Since 1994, a cooler than average spring mean temperature for Australia was observed in only two years.

The seasonally-averaged mean maximum temperature for spring was 1.47°C above the 1961–1990 average (Table 3), the 10th-warmest on record. The mean minimum temperature for Australia was 1.09°C above the 1961–1990 average (Table 4).

Maximum temperatures were above average for nearly all of Australia, and in decile 10 for much of the southeast and around the northern coastline between the Gulf of Carpentaria and the northern Interior District in Western Australia (Fig. 22). Near-average maxima were observed along most of the east coast of Queensland south of the Cape York Peninsula, and in the Victoria River District in the Northern Territory.

Mean minimum temperatures were above to very much above average for most of Australia and in decile 10 for large areas (Table 5), including along the northwest coast and across the South West Land Division in Western Australia, from the Nullarbor to Victoria and through much of western New South Wales and western Queensland, and also in coastal south-eastern

Table 2. Percentage areas in different categories for spring 2017 rainfall. 'Severe deficiency' denotes rainfall at or below the fifth percentile. Areas in decile 1 include those in 'severe deficiency', which in turn includes areas which are 'lowest on record'. Areas in decile 10 include areas which are 'highest on record'. Percentage areas of highest and lowest on record are given to two decimal places because of the small quantities involved; other percentage areas are to one decimal place

Region	Lowest on record (%)	Severe deficiency (%)	Decile 1 (%)	Decile 10 (%)	Highest on record (%)
Australia	0.05	0.4	0.7	14.9	1.44
Queensland	0.22	0.5	0.6	12.4	0.82
New South Wales	0.00	0.1	0.5	0.4	0.00
Victoria	0.00	1.3	2.4	0.0	0.00
Tasmania	0.00	12.7	15.4	0.0	0.00
South Australia	0.00	0.0	0.2	30.6	4.51
Western Australia	0.00	0.4	0.6	16.3	2.03
Northern Territory	0.00	0.2	0.4	15.9	0.06

Table 3. Summary of the mean seasonal maximum temperatures, extremes and rank for Australia and regions for spring 2017. Rank given is 1 (lowest) to 108 (highest) calculated, over the years 1910–2017 inclusive

Region	Highest seasonal mean maximum (°C)	Lowest seasonal mean maximum (°C)	Highest daily maximum temperature (°C)	Lowest daily maximum temperature (°C)	Area-averaged temperature anomaly (°C)	Rank of area-averaged temperature anomaly
Australia	40.0 at Fitzroy Crossing Aero (WA)	8.6 at Thredbo AWS (NSW)	45.1 at Marble Bar (WA) on 22 November	−3.9 at Mount Hotham (Vic.) on 4 September	+1.47	99
Queensland	38.0 at Century Mine	22.2 at Applethorpe	42.8 at Birdsville Airport on 27 September	12.9 at Applethorpe on 1 October	+1.16	94
New South Wales	30.5 Mungindi Post Office	8.6 at Thredbo AWS	41.4 at Wanaaring Post Office on 27 September	−3.3 at Thredbo AWS on 5 September	+2.16	98
Victoria	26.7 at Mildura	9.4 at Falls Creek and Mount Buller	39.6 at Kellalac (Warracknabeal Airport) on 29 November	−3.9 at Mount Hotham on 4 September	+2.00	102
Tasmania	19.8 at Launceston (Ti Tree Bend)	9.0 at Mount Read	34.8 at Scotts Peak Dam on 30 November	−3.0 at Kunanyi (Mount Wellington Pinnacle) on 8 September	+1.59	107
South Australia	31.3 at Moomba Airport	17.7 at Mt Lofty	41.3 at Moomba Airport on 30 November	6.5 at Mt Lofty on 4 September	+1.74	99
Western Australia	40.0 at Fitzroy Crossing Aero	19.1 at Albany	45.1 at Marble Bar on 22 November	10.1 at Rocky Gully on 25 September	+1.49	101
Northern Territory	38.7 at Ngukurr Airport & Bradshaw	30.5 at McCluer Island	43.0 at Lajamanu Airport on 29 October & Walungurru Airport on 30November	16.1 at Alice Springs Airport on 30 September	+1.12	95

Queensland and across Tasmania (Fig. 23). Minima were generally near-average for the Northern Territory south of the Top End and adjacent parts of Western Australia. Below average minima for spring were observed in areas of the eastern Kimberley and northern Alice Springs districts.

Each of the individual months of spring was warmer than average nationally, with warmth most notable for maximum temperatures across the majority of the mainland during September, for both maxima and minima across most of Australia during October, and for both maxima and minima across southern Australia during November. Large areas of eastern Queensland and parts of north-eastern New South Wales observed cooler than average maxima and minima during November.

Table 4. Summary of the mean seasonal minimum temperatures, extremes and rank for Australia and regions for spring 2017. Rank refers to 1 (lowest) to 108 (highest) calculated, over the years 1910–2017 inclusive[12]

Region	Highest seasonal mean minimum (°C)	Lowest seasonal mean minimum (°C)	Highest daily minimum temperature (°C)	Lowest daily minimum temperature (°C)	Area-averaged temperature anomaly (°C)	Rank of area-averaged temperature anomaly
Australia	27.0 at Browse Island (WA)	−1.4 at Liawenee (Tas)	30.5 at Bidyadanga (WA) on 20 October	−9.5 at Perisher Valley & Thredbo AWS (NSW) on 1 September	+1.09	101
Queensland	25.7 at Horn Island	8.9 at Stanthorpe Leslie Parade	29.3 at Thargomindah Airport on 28 November	−4.3 at Stanthorpe on 8 September	+1.51	104
New South Wales	17.4 at Byron Bay (Cape Byron AWS)	0.3 at Thredbo AWS	26.6 at Tibooburra Airport on 28 November	−9.5 at Perisher Valley & Thredbo AWS on 1 September	+1.47	= 104
Victoria	11.6 at Melbourne (Olympic Park)	1.2 at Mount Hotham	24.3 at Scoresby Research Institute on 30 November	−7.5 at Mt Hotham on 5 September	+1.24	= 104
Tasmania	10.9 at Swan Island	−1.4 at Liawenee	20.1 at Cape Sorell on 30 November	−8.0 at Liawenee on 1 September	+0.68	102
South Australia	16.5 at Moomba Airport	7.9 at Yongala	27.1 at Noarlunga on 22 November	−2.3 at Renmark Aero on 17 September & Keith (Munkora) on 4 November	+1.26	101
Western Australia	27.0 at Browse Island	8.1 at Wandering	30.5 at Bidyadanga on 20 October	−5.1 at Eyre on 14 September	+0.92	102
Northern Territory	26.6 at McCluer Island	13.4 at Arltunga	30.2 at Bradshaw on 22 October	0.0 at Arltunga on 2 and 15 September	+0.49	79

Table 5. Percentage areas in different categories for spring 2017. Areas in decile 1 include those which are 'lowest on record'. Areas in decile 10 include areas which are 'highest on record'. Percentage areas of highest and lowest on record are given to two decimal places because of the small quantities involved; other percentage areas are to one decimal place

Region	Maximum temperature				Minimum temperature			
	Lowest on record	Decile 1	Decile 10	Highest on record	Lowest on record	Decile 1	Decile 10	Highest on record
Australia	0.00	0.0	42.9	0.09	0.00	0.0	49.1	1.87
Queensland	0.00	0.0	16.4	0.00	0.00	0.0	69.6	0.82
New South Wales	0.00	0.0	57.4	0.00	0.00	0.0	64.3	0.00
Victoria	0.00	0.0	89.9	0.00	0.00	0.0	84.4	27.75
Tasmania	0.00	0.0	100.0	6.17	0.00	0.0	81.1	0.00
South Australia	0.00	0.0	58.7	0.00	0.00	0.0	55.1	6.55
Western Australia	0.00	0.0	49.6	0.12	0.00	0.0	48.3	0.00
Northern Territory	0.00	0.0	33.3	0.00	0.00	0.0	1.6	0.00

Several periods of exceptional warmth contributed to the very warm spring. High temperature records for September were set in Victoria, New South Wales and Queensland during the last week of that month associated with a favourable synoptic situation of Tasman Sea high pressure systems and troughs over central Australia[13]. A strong blocking high in the Tasman was also responsible for an extended period of very warm weather during November across south-eastern Australia, during which significant records for runs of consecutive warm days were set[14].

[12]A subset of the full temperature network is used to calculate the spatial averages and rankings shown in Table 3 (maximum temperature) and Table 4 (minimum temperature); this dataset is known as ACORN-SAT (see http://www.bom.gov.au/climate/change/acorn-sat/ for details). These averages are available from 1910 to the present. As the anomaly averages in the tables are only retained to two decimal places, tied rankings are possible. Rankings marked with "=" denote tied rankings. ACORN-SAT temperatures are also used for Table 5.

[13]Bureau of Meteorology, Special Climate Statement 62, Exceptional September heat in eastern Australia. Available at http://www.bom.gov.au/climate/current/statements/scs62.pdf.

[14]Bureau of Meteorology, Special Climate Statement 63, A prolonged warm spell in Tasmania and Victoria. Available at http://www.bom.gov.au/climate/current/statements/scs63.pdf.

(*a*)

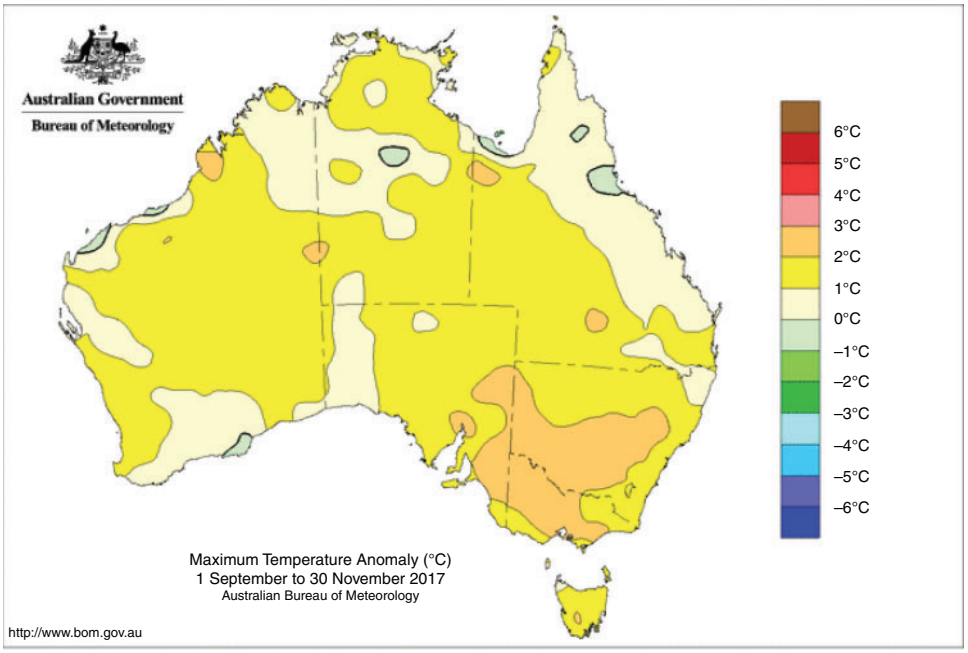

(*b*)

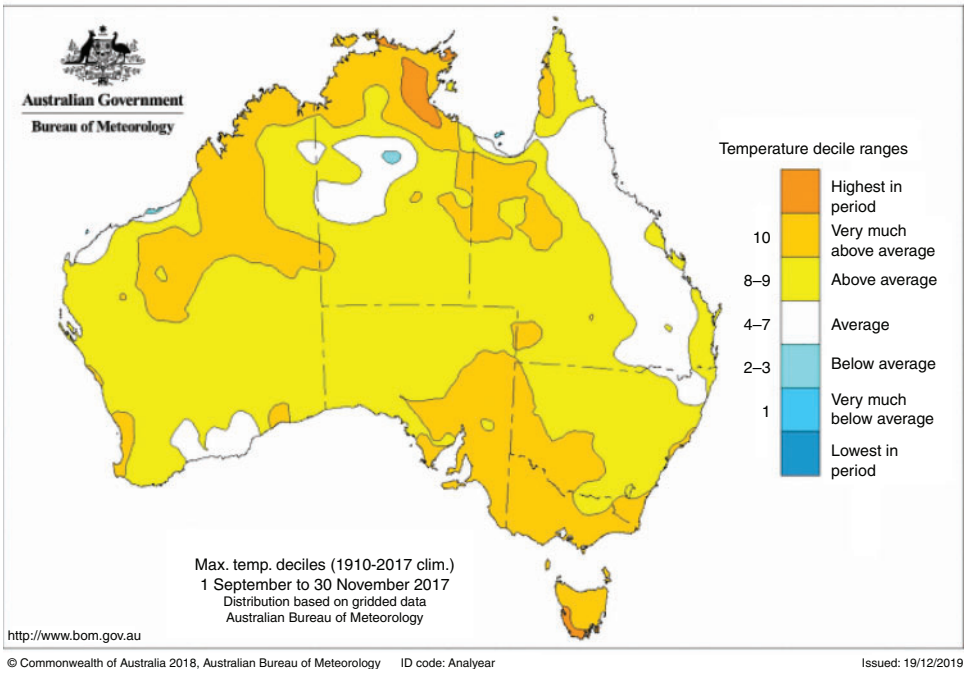

Fig. 22. (*a*) Maximum temperature anomalies (°C) for spring 2017; based on average climate 1961–1990. (*b*) Maximum temperature deciles for spring 2017; decile ranges based on grid-point values over the springs 1910–2017.

(*a*)

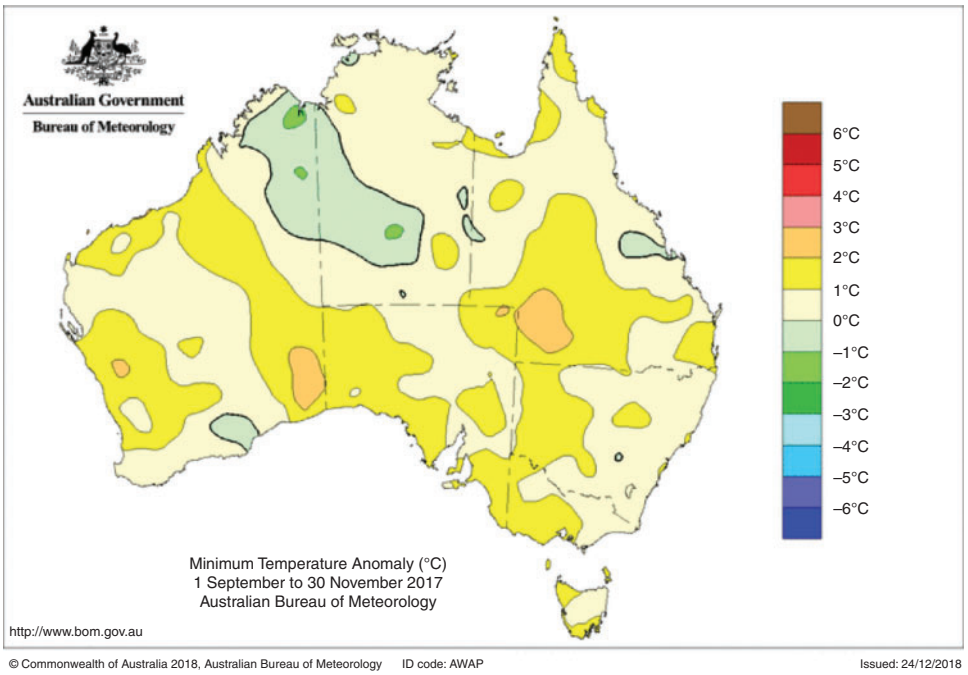

(*b*)

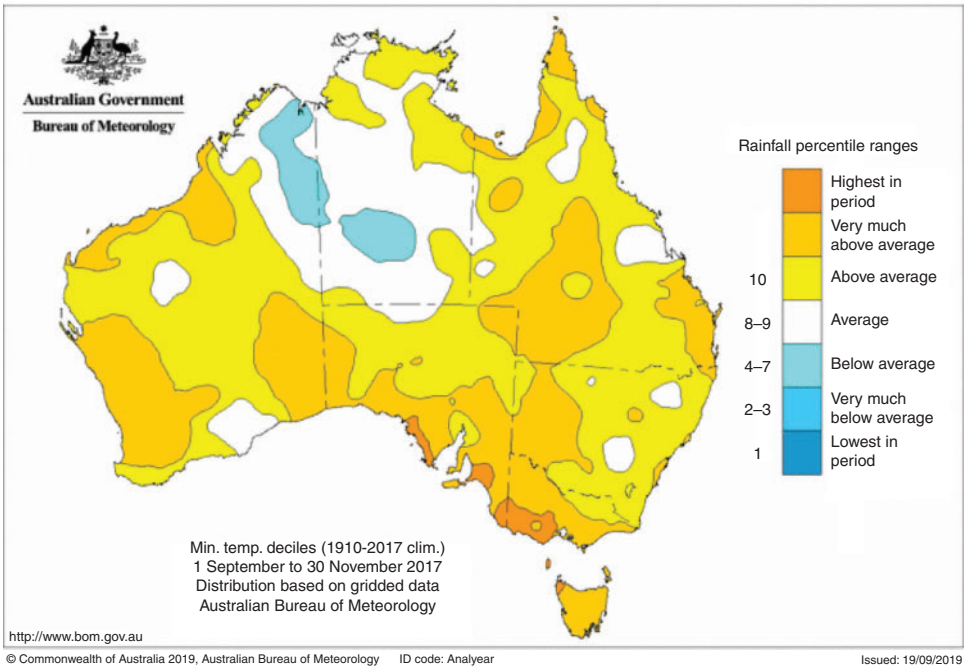

Fig. 23. (*a*) Minimum temperature anomalies (°C) for spring 2017; based on average climate 1961–1990. (*b*) Minimum temperature deciles for spring 2017; decile ranges based on grid-point values over the springs 1910–2017.

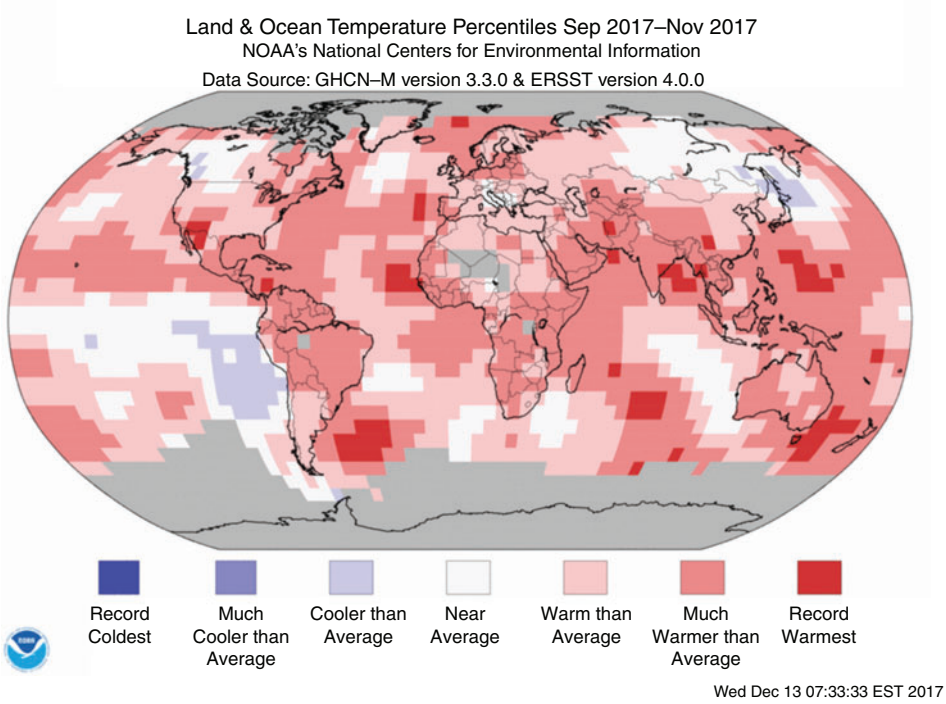

Fig. 24. Mean temperature percentiles for September–November 2017, using all available data 1880–present (source: National Centers for Environmental Information).

9 Southern hemisphere

Spring was significantly warmer than average over most parts of the southern hemisphere[15]. The seasonally-averaged mean temperature was only cooler than average for an area of the South Atlantic Ocean adjacent to the west coast of South America (Fig. 24). Warmest on record temperatures for spring were analysed over some areas, including in the Tasman Sea, to the southeast of South America and in part of the central southern Pacific Ocean.

Averaged over the southern hemisphere as a whole, it was one of the warmest springs on record. Of the three major global datasets, spring 2017 ranked as the equal-third-warmest on record for the southern hemisphere in the National Oceanic and Atmospheric Administration (NOAAGlobalTemp[16]) dataset (Smith *et al.* 2008), the sixth-warmest in the National Air and Space Administration (NASA) US Goddard Institute of Space Studies (GISTEMP[17]) dataset (Hansen *et al.* 2010, and Lenssen *et al.* 2019) and the equal-twelfth-warmest in the United Kingdom Meteorological Office Hadley Centre/Climatic Research Unit, University of East Anglia (HadCRUT4[18]) dataset (Morice *et al.* 2012).

The differences in ranks between the three datasets reflect the different methods they use for assessing temperatures over data-sparse land areas, particularly Antarctica, while the uncertainty in temperature measurements is typically greater in the southern than the northern hemisphere due to the lower data density.

Temperatures in spring 2017 were above the 1981–2010 average over most southern hemisphere land areas, and were below the 1981–2010 average over parts of the eastern Indian Ocean, much of the western half of the South Pacific Ocean, for areas of the South Atlantic Ocean close to South America and to either side of far southern Africa. However, cool anomalies were generally weak and were within one degree of the 1981–2010 average except for some isolated grid cells in the tropics of the eastern Pacific – consistent with developing La Niña. Warm anomalies were also within one degree of the 1981–2010 average for large areas, but exceeded +1°C over parts of western and south-eastern Australia, some areas of the western and southern Pacific Ocean and a few other scattered grid cells (Fig. 25).

Fig. 26 shows global rainfall patterns for spring 2017. As analysed by the GPCC[19].

[15]Please note, NCEI use a different methodology for assigning climatological rankings, most importantly percentiles are calculated against data from 1880, not 1910 as for the Australian temperature maps in Section 8, nor 1900 as for SST deciles in Fig. 10. See details of NCEI's climatological rankings at https://www.ncdc.noaa.gov/monitoring-references/dyk/global-mntp-percentiles.

[16]https://www.ncdc.noaa.gov/data-access/marineocean-data/noaa-global-surface-temperature-noaaglobaltemp

[17]https://data.giss.nasa.gov/gistemp/

[18]https://www.metoffice.gov.uk/hadobs/hadcrut4/

[19]https://www.dwd.de/EN/ourservices/gpcc/gpcc.html

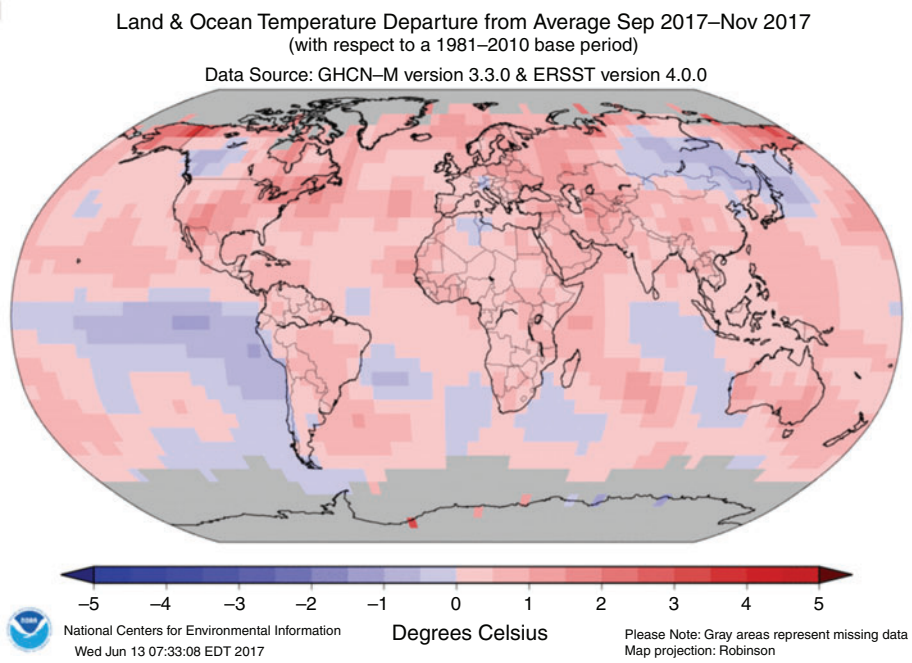

Fig. 25. Mean temperature anomalies (°C) from a 1981–2010 base period for September–November 2017 (source: National Centers for Environmental Information).

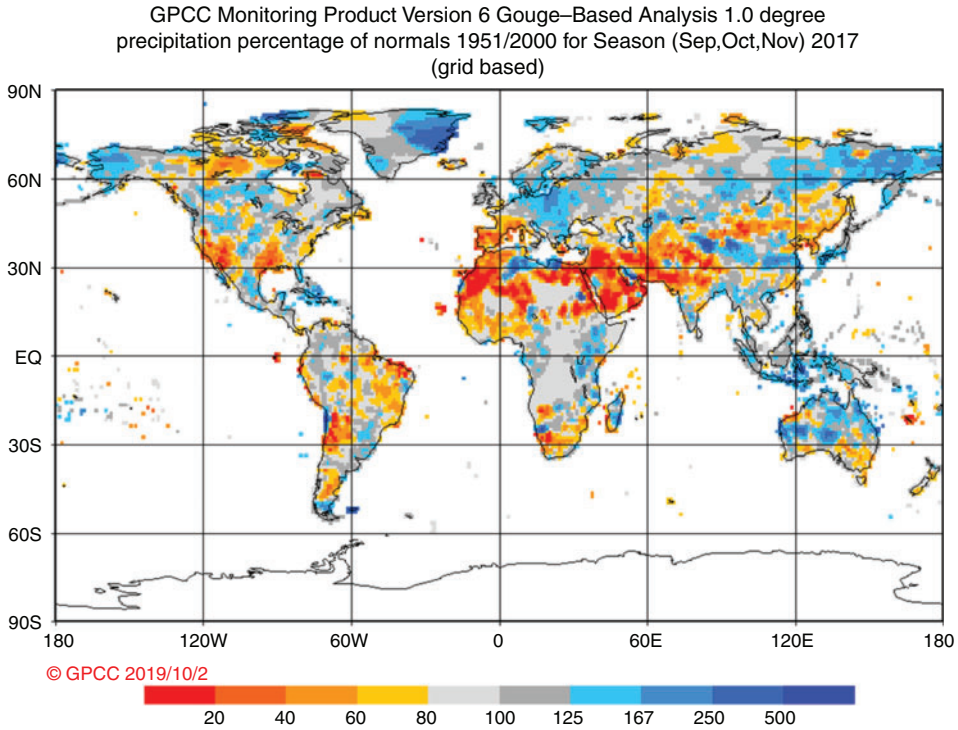

Fig. 26. Precipitation as a percentage of the 1951–2000 average for September–November 2017 (source: Global Precipitation Climatology Centre).

September–November rainfall was below average for the far south of Africa, much of southern Australia, New Zealand and large parts of South America – rainfall was particularly low around Bolivia and the north coast of Brazil.

Precipitation was above average for the southern tip of South America, some areas in south-eastern Brazil and along the coast near the border of Peru and Chile. Rainfall was also above average for some areas of eastern Africa between Ethiopia and Mozambique, and for parts of Madagascar. Rainfall was very much above average for parts of Indonesia and the Maritime Continent, and above average for parts of western, central and northern Australia.

Conflicts of interest

The authors declare that they have no conflicts of interest.

Acknowledgements

Thanks to Bernard Chapman and Acacia Pepler, and their canine and feline assistants respectively, for their helpful comments on the manuscript. This research did not receive any specific funding.

References

Donald, A., Meinke, H., Power, B., Wheeler, M., and Ribbe, J. (2004). Forecasting with the Madden-Julian Oscillation and the applications for risk management. In 'International Crop Science Congress (ICSC 2004): New Directions for a Diverse Planet, 26 September–1 October 2004, Brisbane, Australia'. Available at http://www.cropscience.org.au/icsc2004/poster/2/6/1362_donalda.htm

Hansen, J., Ruedy, R., Sato, M., and Lo, K. (2010). Global surface temperature change. *Rev. Geophys.* **48**, RG4004. doi:10.1029/2010RG000345

Hendon, H., Thompson, D. W. J., and Wheeler, M. C. (2007). Australian rainfall and surface temperature variations associated with the southern hemisphere annular mode. *J. Climate* **20**, 2452–2467. doi:10.1175/JCLI4134.1

Huang, B., Thorne, P. W., Banzon, V. F., Boyer, T., Chepurin, G., Lawrimore, J. H., Menne, M. J., Smith, T. M., Vose, R. S., and Zhang, H.-M. (2017). Extended Reconstructed Sea Surface Temperature, Version 5 (ERSSTv5): upgrades, validations and intercomparisons. *J. Climate* **30**, 8179–8205. doi:10.1175/JCLI-D-16-0836.1

Jones, D. A., Wang, W., and Fawcett, R. (2009). High-quality spatial climate data-sets for Australia. *Aust. Met. Oceanogr. J.* **58**, 233–248. doi:10.22499/2.5804.003

Kanamitsu, M., Ebisuzaki, W., Woollen, J., Yang, S.-K, Hnilo, J. J., Fiorino, M., and Potter, G. L. (2002). NCEP-DOE AMIPII Reanalysis (R-2). *Bull. Amer. Meteor. Soc.* **83**, 1631–1643. doi:10.1175/BAMS-83-11-1631

Kuleshov, Y., Qi, L., Fawcett, R., and Jones, D. (2009). Improving preparedness to natural hazards: Tropical cyclone prediction for the Southern Hemisphere. *Adv. Geosci.* **12**(Ocean Science), 127–143. doi:10.1142/9789812836168_0010

Lenssen, N., Schmidt, G., Hansen, J., Menne, M., Persin, A., Ruedy, R, and Zyss, D. (2019). Improvements in the GISTEMP uncertainty model. *J. Geophys. Res. Atmos.* **124**(12), 6307–6326. doi:10.1029/2018JD029522

Madden, R. A., and Julian, P. R. (1971). Detection of a 40–50 day oscillation in the zonal wind in the tropical Pacific. *J. Atmos. Sci.* **28**, 702–708. doi:10.1175/1520-0469(1971)028<0702:DOADOI>2.0.CO;2

Madden, R. A., and Julian, P. R. (1972). Description of global-scale circulation cells in the tropics with a 40–50 day period. *J. Atmos. Sci.* **29**, 1109–1123. doi:10.1175/1520-0469(1972)029<1109:DOGSCC>2.0.CO;2

Madden, R. A., and Julian, P. R. (1994). Observations of the 40–50 day tropical oscillation: a review. *Mon. Wea. Rev.* **122**, 814–837. doi:10.1175/1520-0493(1994)122<0814:OOTDTO>2.0.CO;2

Martin, D. J., and Tobin, S. (2019). Seasonal climate summary for the southern hemisphere (winter 2017): exceptionally warm days for Australia. *J. South. Hemisph. Earth Syst. Sci.* **69**, 331–350. doi:10.1071/ES19012

Morice, C. P., Kennedy, J. J., Rayner, N. A., and Jones, P. D. (2012). Quantifying uncertainties in global and regional temperature change using an ensemble of observational estimatesL the HadCRUT4 dataset. *J. Geophys. Res.* **117**, D08101. doi:10.1029/2011JD017187

Mullen, C. (2009). Seasonal climate summary southern hemisphere (summer 2008–09): a weak, brief La Niña returns. Bumper wet season in tropical Australia; exceptional heatwaves in southeastern Australia. *Aust. Met. Oceanogr. J.* **58**, 275–284. doi:10.22499/2.5804.006

Qi, L. (2009). Seasonal climate summary southern hemisphere (spring 2008): La Niña pattern returning across the equatorial Pacific. *Aust. Met. Oceanogr. J.* **58**, 199–208. doi:10.22499/2.5803.005

Rosemond, K., and Tobin, S. (2018). Seasonal climate summary for the southern hemisphere (autumn 2016): El Niño slips into neutral and a negative Indian Ocean Dipole develops. *J. South. Hemisph. Earth Syst. Sci.* **68**, 124–146. doi:10.22499/3.6801.007

Saji, N. H., Goswami, B. N., Vinayachandran, P. N., and Yamagata, T. (1999). A dipole mode in the tropical Indian Ocean. *Nature* **401**, 360–363. doi:10.1038/43854

Smith, T. M., Reynolds, R. W., Peterson, T. C., and Lawrimore, J. (2008). Improvements to NOAA's Historical Merged Land–Ocean Surface Temperature Analysis (1880–2006). *J. Climate* **21**, 2283–2296. doi:10.1175/2007JCLI2100.1

Trewin, B. C. (2013). A daily homogenized temperature data set for Australia. *Int. J. Climatol.* **33**, 1510–1529. doi:10.1002/JOC.3530

Trewin, B. C. (2018). The Australian Climate Observations Reference Network – Surface Air Temperature (ACORN-SAT) version 2. Bureau Research Report – 032. Available at http://www.bom.gov.au/research/publications/researchreports/BRR-032.pdf

Troup, A. (1965). The Southern Oscillation. *Quart. J. Roy. Met. Soc.* **91**, 490–506. doi:10.1002/QJ.49709139009

Wang, G., and Hendon, H. H. (2007). Sensitivity of Australian rainfall to inter-El Niño variations. *J. Climate* **20**, 4211–4226. doi:10.1175/JCLI4228.1

Wheeler, M., and Hendon, H. (2004). An All-Season Real-Time Multivariate MJO Index: Development of an Index for Monitoring and Prediction. *Mon. Wea. Rev.* **132**, 1917–1932. doi:10.1175/1520-0493(2004)132<1917:AARMMI>2.0.CO;2